Comprehensive Summaries of Uppsala Dissertations
from the Faculty of Science and Technology 578

Tuning Electron Transfer Reactions by Selective Excitation in Porphyrin –Acceptor Assemblies

BY

MIKAEL ANDERSSON

ACTA UNIVERSITATIS UPSALIENSIS
UPPSALA 2000

Dissertation for the Degree of Doctor of Philosophy in Physical Chemistry presented at Uppsala University in 2000

ABSTRACT

Andersson, M. 2000. Tuning Electron Transfer Reactions by Selective Excitation in Porphyrin - Acceptor Assemblies. Acta Universitatis Upsaliensis. *Comprehensive Summaries of Uppsala Dissertations from the Faculty of Science and Technology* 578. 58 pp. Uppsala. ISBN 91-554-4843-7.

This thesis concerns electron transfer reactions from different excited states in porphyrins, and the effect of changing the energy of the link connecting the donor and acceptor. Photoinduced electron transfer, and subsequent processes were studied using ultrashort laser pulses and nanosecond laser flash photolysis.

Excitation of Zn(II)-porphyrins in the Soret band lead to population of the higher lying S_2 state. The lifetime and transient absorption spectrum was measured for the S_2 state. When an electron acceptor was attached to the Zn(II)-porphyrin, either as an ion pair, or covalently bound through an amide link, electron transfer was found to compete with S_2 to S_1 relaxation. In the ion pair, electron transfer was faster than 200 fs, with a lifetime of the charge separated state of 1.3 ps. Further, in the covalently linked dyad, the Zn(II) porphyrin triplet state was repopulated from a charge transfer state.

In [2]-rotaxanes, the Zn(II) porphyrin donor (ZnP) and Au(III) porphyrin acceptor (AuP^+) are not connected by a direct covalent link. Selective excitation of either the ZnP or the AuP^+ resulted in rapid electron transfer from the ZnP to the AuP^+. The bis-phenanthroline link connecting the different porphyrins was changed by coordination of Cu(I) or Ag(I). Electron transfer from the ^{1}ZnP singlet was unaffected by coordination of either Ag(I) or Cu(I), while electron transfer to the $^3AuP^+$ triplet was in the Ag(I) link found to occur by an enhanced superexchange, and by a sequential mechanism in the Cu(I) coordinated link.

Mikael Andersson, Department of Physical Chemistry, Uppsala University, Box 532, SE-751 21 Uppsala, Sweden

ISSN 1104-232X
ISBN 91-554-4843-7

Printed in Sweden by Akademitryck AB, Edsbruk, 2000

List of Papers

This thesis is based on the papers listed below. They are referred to in the summary by their roman numbers.

I **Photoinduced Electron Transfer Reactions in a Porphyrin-Viologen Complex: Observation of S_2 to S_1 Relaxation and Electron Transfer from the S_2 State**
Mikael Andersson, Jan Davidsson, Leif Hammarström, Jouko Korppi-Tommola and Timo Peltola
Journal of Physical Chemistry B, **1999**, *103*, 3258

II **Photoinduced Electron Transfer from a Higher Excited State of a Porphyrin in a Zinc Porphyrin-Ruthenium(II) tris-Bipyridine Dyad.**
Denis LeGourriérec, Mikael Andersson, Jan Davidsson, Emad Mukhtar, Licheng Sun and Leif Hammarström
Journal of Physical Chemistry A, **1999**, *103*, 557

III **Porphyrin-containing [2]-Rotaxanes: Metal Coordination Enhanced Superexchange Electron Transfer between Noncovalently Linked Chromophores**
Mikael Andersson , Myriam Linke, Jean-Claude Chambron, Jan Davidsson, Valérie Heitz, Jean-Pierre Sauvage and Leif Hammarström
Journal of the American Chemical Society, **2000**, *122*, 3526

IV **Tuning Long Range Electron Transfer Reactions Between Non-covalently Linked Porphyrins in [2]-Rotaxanes: From a Superexchange to a Sequential Mechanism?**
Mikael Andersson, Myriam Linke, Jean-Claude Chambron, Jan Davidsson, Valérie Heitz, Leif Hammarström and Jean-Pierre Sauvage

In manuscript

V **Electron Transfer from the Higher Excited S_2 State of a Porphyrin in a Zn(II)tetratolylporphyrin-Ru(bpy)$_3^{2+}$ Dyad**
Mikael Andersson, Tilmann Häupl, Jan Davidsson, Licheng Sun and Leif Hammarström

In manuscript

Contents

1. Introduction

This introduction is intended to give the non scientist an idea of the work presented. The thesis consists of two chapters of general information relevant for the discussion in the presented work; porphyrins as photosensitisers and electron transfer theory. Further, a chapter is devoted to describe and discuss the instrumentation used in different experiments. In two chapters I present and discuss the major results obtained in the electron transfer reactions I have studied.

The main issue in this thesis is electron transfer reactions. The most important electron transfer reactions for the life on this planet are the ones that occur in the photosynthetic reactions in the green plants. Molecules absorb the energy of the sunlight, and the primary chemical reaction is electron transfer from a unit of excited chlorophylls to an electron acceptor. Electron transfer occurs in a series of subsequent reactions, eventually leading to the formation of ATP, and further to the build up of carbohydrates, proteins and fat [1]. The chlorophyll that initially lost an electron in the excited state reaction, receives an electron from another donor, and can go through another excitation and electron transfer cycle. The electron from the donor comes from water molecule(s), attached to a manganese cluster. After four completed cycles with removal of electrons from the water, oxygen is released as a bi-product. On the other end of the complicated electron transfer system, CO_2 is reduced to build carbohydrates, proteins and fat. The "motor" that drives this electron pump is the photosynthetic reaction center, and the fuel for the motor is the sunlight.

It has long been the desire to be able to mimic the natural photosynthesis in order to harvest the solar energy into chemically stable products. In today's times of increasing air pollution, ozone holes that grow and threatening green house effects, the idea of using solar energy is a highly urgent issue. In an artificial photosynthetic system, one wishes to control the rate and yield in each chemical reaction. Further, the total energy yield should be as high as possible. In order to accomplish this, one has to understand the mechanisms that control each individual step in the whole process.

Furthermore, in electronics, the need for smaller and smaller devices has created an interest in building switches and "machines" on a molecular scale.[2-5] Light driven reactions could be used for storage of information. Since electron transfer reactions can occur within a few femtoseconds, such small devices could also work fast.

This thesis concerns mainly two different aspects of electron transfer: reactions from higher excited states in porphyrins, and the effects of varying the properties of a link that connects an electron donor with an electron acceptor. A common feature in the studies I present here is the selectivity in the excitation. Different photochemical and photophysical events could be started by irradiation of light of different wavelengths.
Electron transfer from higher excited states can be used in the design of optoelectronic devices, as shown schematically in figure 1. By selective excitation of the Zn- porphyrin with light of different wavelengths (red or blue),

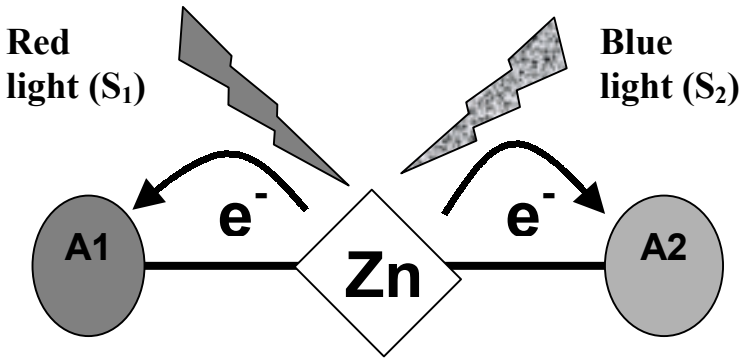

Figure 1

different excited states (S_1 and S_2) are initially populated, and electron transfer to either the A_1 or the A_2 acceptor can be accomplished in a controlled way.

Furthermore, by electron transfer reactions from a higher excited state, more energy could in principle be harvested in an initial photosynthetic reaction, since products with higher energy can be formed in the electron transfer reaction. Thus electron transfer from higher excited state might be of relevance both in the design of artificial photosynthetic systems, and in the design of molecular switches and "machines".

For electron transfer reactions to occur, the electron donor and acceptor molecules must not be totally isolated from each other. An electronic coupling is needed for the electron to be transferred. Even at fairly small distances, the

direct coupling becomes small, and the electron transfer is slow. However, the medium between the donor and acceptor molecule can promote the electron transfer, by increasing the electronic coupling of the donor and acceptor. Depending on the properties of the intervening medium, the electron transfer between the donor and acceptor molecules can occur by two different mechanisms; either by a sequential, electron hopping or by a superexchange mechanism [6-8]. In chapter 6, electron transfer reactions are presented for a series of [2]-rotaxanes. The donor and acceptor molecules are the same, while the link between them was modified by coordination of a metal cation. The main findings in these models were that modifying the energy levels of the link could change the electron transfer mechanisms from a superexchange to a sequential mechanism.

2. Porphyrins as photosensitisers.

2.1 General properties

Porphyrins and porphyrin-type molecules are abundant in nature, and they play important roles in a large number of different natural occurring processes. For example, electron transfer and energy transfer processes in the photosynthesis, oxygen binding in heme proteins and electron transfer in the respiratory chain.[9] The intricate balance of oxygen coordination in the heme/myoglobin molecules, providing the base of oxygen transport from the lungs to the muscles is an example of axial coordination by a metal. In the green plant photosynthetic system, the energy of the sunlight is collected efficiently by stacked porphyrins in the antenna complexes, and the energy is transferred to the reaction center, the P680 unit.[1,9] The porphyrins in the antennas are strongly coupled in a defined geometry, and the excited states have exciton character. A series of electron transfer reactions starting with the oxidation of the excited P680 unit, finally lead to the reduction of a quinone. The energy is finally stored as ATP. Molecules from the porphyrin family have been used in a large number of studies; in model systems for solar energy conversion in artificial photosynthesis[10,11] in photodynamic therapy [12], as models for general electron and energy transfer studies [10,11], as sensitisers for various photoactive switches and supramolecular devices [2-5,10]. The porphyrin structure, with the possibility of metal binding and substitution offers good possibilities to tune properties such as solubility, redox potentials, excited state energies and lifetimes. The porphyrins can be subject to various substitutions on the macrocycle, introducing several brigding links to electron and energy donors and acceptors, without severely affecting the photophysical and photochemical properties, as well as changing solubility properties and introducing sterical constraints. Further, porphyrins can coordinate a number of different metals by the four central nitrogens to form metal porphyrins [13,14]. Depending of the type of coordinated metal, new properties can be introduced; the redox potentials, and excited state energies and lifetimes can be finely tuned, and ligands can be axially bound. A naturally occurring porphyrine inside a protein is subject to interaction with several parts of the protein by direct covalent bonding, by hydrogen bonds and by electrostatic interactions. A small configuration change of the protein matrix might lead to changed properties of the porphyrin. In photosynthetic reactions, this offers a tool for controlling the direction and rates of electron transfer reactions. In many porphyrins, the ground state oxidation potentials are favourable for photosynthetic reactions [13-16]. The energy difference between the ground state and the lowest singlet excited state is for regular porphyrins around 2 eV, [13,17,18] while the higher lying singlet state is close to 3 eV higher than the ground state. The absorption of light in the visible range is strong, making porphyrins good candidates for harvesting

of the solar energy. There are many types of porphyrins, both naturally occuring and synthetical, and I will in this chapter describe the characteristics of the metalated porphyrins used in my work. Below is given the basic structure of the free base porphyrin (porphine) and metal porphyrin, with numbering of the different positions of the macrocycle.

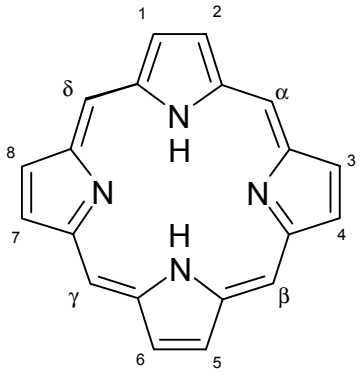

Free base porphyrin

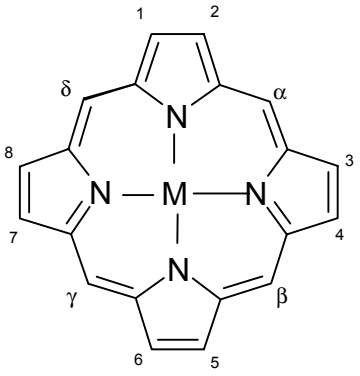

Metal porphyrin

The central ring of the porphyrins consists of conjugated pi electrons, with an inner ring of 18 electrons. Thus, a 4n+2 pi electron system makes the ring aromatic. In the free base porphyrin, two of the central nitrogen atoms bind to protons. The protons can be removed and replaced by a metal cation, forming a metal porphyrin. A classification of the different metal porphyrins can be made according to their ground state absorption properties, but the porphyrins can also be divided into two subgroups based on the substitutions. [13,17] The four methine carbons in the porphyrin skeleton are denoted meso positions, and porphyrins with substituents on these positions are called meso- or β substituted, while porphyrins with substituents on the pyrrole ring are called α porphyrins.

2.2 Ground state absorption

By the ground state absorption spectra, the porphyrins are classified as regular or irregular. The absorption spectrum of a regular porphyrin are determined essentially by the pi orbitals of the porphyrin macrocycle, whereas an irregular porphyrin displays absorption features with contributions also from the metal d-orbitals. In regular porphyrins, the absorption spectra is characterised by a strong transition centered around 420 nm, often denoted the B or the Soret band and weaker transitions in 500-650 nm range, often denoted the Q bands.[17] In the free base porphyrins, the Q bands can be seen as four distinct bands. These are the $Q_x(0,0)$ and $Q_y(0,0)$, and corresponding vibrational overtones $Q_{x,y}(1,0)$.
If a closed shell metal ion, like Zn^{2+} is coordinated to the porphyrin, the two states corresponding to the x,y transitions in the free base porphyrin become degenerate, and the absorption from the Q_x and Q_y transitions are overlapping. Thus, the absorption of the Q bands will be reduced to two bands; Q(1,0) and Q(0,0).

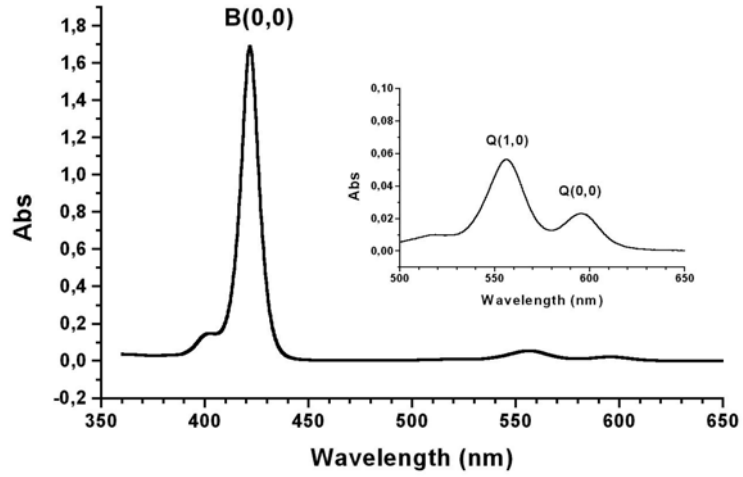

Figure 2.1 Absorption spectrum of ZnTPPS i water. The strong absorption centered at 421 nm is the Soret band. Inset show the Q(1,0) and Q(0,0) bands.

The absorption spectra in the visible range has been succesfully described by a four orbital model [19]. The four orbitals involved are the HOMO-1, HOMO, LUMO and LUMO+1, which are π and π^* orbitals from the porphyrin structure. The Soret band consist of transitions involving the a_{1u} and the e_g orbitals, while the Q bands are described by transitions involving the a_{2u} and the e_g orbitals.

Binding of a (closed shell) metal does not give rise to new transitions, but interaction with the metal d orbitals will cause a shift of the π orbitals on the porphyrin ring. The a_{1u} MO has nodes on the nitrogens, and do not interact directly with the metal orbitals, while the a_{2u} MO will be shifted by interaction with metal orbitals.[13] Thus, metalation of the porphyrin will change the Q bands by degeneration of the two bands and also by a change of the energy. Further, the intensity of the Q transition can be correlated with the interaction with the bound metal [13]. The four methine carbons in the porphyrin skeleton are denoted meso positions, and the a_{1u} orbital has nodes at these positions while the a_{2u} orbital places considerable electron density.[13] Hence, substitutions on the meso positions are likely to affect the absorption spectrum mostly in the Q bands. The β carbons at the pyrrole rings have more charge in the a_{1u} orbital than in the a_{2u}, and therefore the absorption spectrum is expected to be changed in the Soret band upon substitution on the pyrrole rings.

.

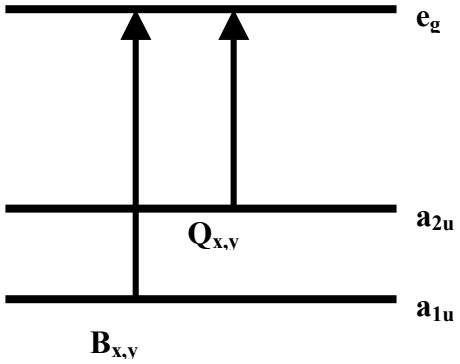

Figure 2.2. The four orbital model. The LUMO and LUMO+1 orbitals are the degenerate e_g orbitals

2.3 Excited states properties

Figure 2.3 is a Jablonski diagram of the ground state (S_0) and the first and second excited states (S_1, S_2). Excitation in the Soret band creates the second excited state, S_2. In some porphyrins, emission from the S_2 state can be seen, with emission peak around 430 nm [13,20-24] The highly allowed S_0 to S_2

transition and hence also the S_2 to S_0 transition, together with a short natural radiative lifetime of S_2, allows the S_2 emission decay to compete with the nonradiative internal conversion to the S_1 state. In Zn porphyrins, the lifetime of S_2 has been measured by fluorescence up conversion [23,24], transient absorption [**I,II,V**], spectral hole burning [25] and fluescence quantum yield comparison [20,26] yielding lifetimes of 0.2 to 3.6 ps. The S_2 lifetime of water soluble ZnTPPS and a β-substituted ZnTTP were studied by transient absorption in paper I, II and V. Vibrational relaxations within the S_2 and S_1 state has been found to occur considerably faster than the S_2 to S_1 internal conversion

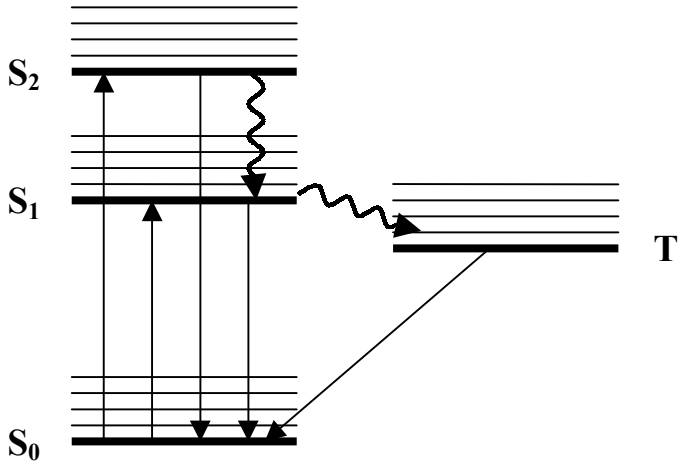

Figure 2.3 Jablonski diagram, showing optical transitions, internal conversions and intersystem crossing in a regular porphyrin.

[23]. In free base porphyrins, the S_2 lifetime is reduced, and no emission from S_2 has been detected.

In Zn porphyrins, the observed lifetime of the S_1 state are typically 2 ns. Intersystem crossing to the triplet state occurs with a quantum yields typically 70% or higher [13]. Thus, the observed lifetime of the S_1 state reflects mostly the rate of intersystem crossing. The fluorescence quantum yield in free base

and Zn porphyrins varies between a few and up to 10 percent, depending on solvent and environment [13]. The sum of the quantum yields for fluorescence and intersystem crossing is for free base and regular porphyrins close to 1, indicating minor contributions from other non radiative relaxation processes.[13] The emission spectra of Zn porphyrins display two characteristic peaks in the 600 to 700 nm region. In free base porphyrins, the lifetime of the S_1 state is longer than for the corresponding Zn porphyrin: For ZnOEP the S_1 lifetime is 2.3 ns, whereas the H_2OEP has S_1 lifetime of 18 ns [13]. In Au(III) porphyrins, the lifetime of the S_1 state is considerably reduced. [13,27,28] Due to a strong spin orbit coupling, a rapid (<3ps) formation of the triplet state occurs. At room temperaure, the Au(III) porphyrin in paper III, IV do not emit light.

Typical lifetimes of the triplet state of Zn porphyrins at room temperature is from a few hundred μs to a few ms. Phosphoresce is not observed in solutions of regular porphyrins at room temperature, while at 77K the phosphorescence quantum yield of Zn porphyrins are typically a few percent. In some substituted Zn porphyrins, dramatically shortened triplet lifetimes has been observed, with a proposed conformational change to a more nonplanar macrocycle [29, **IV**]. The triplet dynamics, which were observed by a change in the transient absorption spectrum of the triplet, with red shift of the transient peak from 456 to 464 nm, occurred with a lifetime of 100 ns for a pyrrol-substituted Zn porphyrin in DMF [**IV**]. The triplet lifetime of the Au(III) porphyrin in III and IV was found to be 2.0 ns.

The excited state absorption spectra of the S_2, S_1 and the lowest triplet states in regular porphyrins are characterised by a strong ground state bleaching corresponding to the Soret band, and weaker bleaching from the Q bands. In Zn porphyrins, stimulated emission from the S_2 state shifts the bleach of the Soret band compared with the S_1 state. [**I,II,V**] Between the Soret and the Q bands, a broad absorption is seen. The absorption in this region displays features suggesting the presence of several overlapping absorption peaks, with a peak around 460 nm, and a broad shoulder in the 490-540 nm region [**I,III,IV**]. On the red side of the Q bands, a broad, featureless absorption is seen that stretches into the NIR region. At higher energies than the Soret band, the absorption is stronger than in the ground state, resulting in positive transient absorption. Figure 2.4 displays a transient absorption spectra for ZnTPPS, upon excitaion in the Soret band. At early times, the transient absorption is mainly the difference between the S_2 state and the ground state, while after 10 ps, the spectra is the difference between the S_1 and ground states. In the steep region between the Soret bleaching centered around 420 nm, and the excited state absorption peak at 460 nm, there is a clear difference between the S_2 and the S_1 state transient absorption. At 435 nm, the S_2 state displays a strong bleaching in the transient

absorption, while the S_1 state displays very small or no net transient absorption. The origin of this spectral difference might be explained by a combined effect of smaller excited state exctinction coefficien of the S_2 state and the presence of stimulated emission. The excited state absorpion of the S_2 state was found to be smaller than that for S_1 in the whole range between the Soret and Q bands, and the relaxation from S_2 to S_1 can be seen in this region as a rise of the transient absorption. On the blue side of the Soret band, however, the excited state absorption of the S_2 state is larger than for the S_1 state, and both are larger than

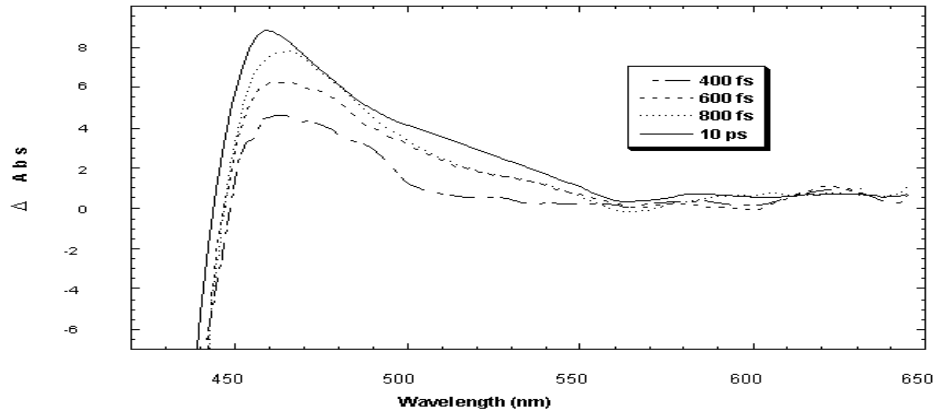

Figure 2.4 Transient absorption spectra of ZnTPPS, taken at various time delays upon Soret band excitation.

the ground state absorption. Thus, S_2 to S_1 relaxation can be seen as a decay of the transient absorption. Figure 2.5 a, b show transient absorption traces of S_2 to S_1 relaxation for ZnTPPS, measured at two different wavelengths.

2.4 Redox properties

Free base and metal porphyrins can be reversibly reduced or oxidised. The metal present interacts with the porphyrin orbitals, and the redox potentials can be varied by the use of different metals. For the water soluble $ZnTPPS^{4-}$ the potential for the ground state oxidation

$$ZnTPPS^{3-} + e^- \rightarrow ZnTPPS^{4-} \qquad (1)$$

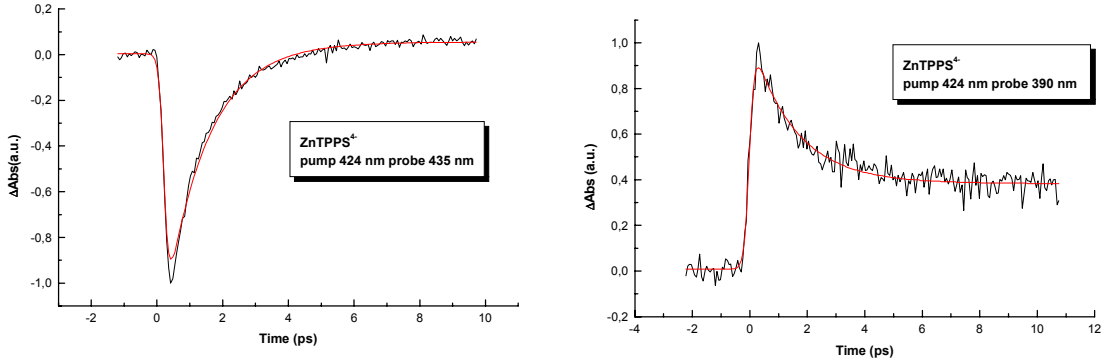

Figure 2.5 Transient absorption changes of ZnTPPS, upon excitation in the Soret band.

is 0.87 V vs NHE, while the ground state reduction reaction

$$ZnTPPS^{4-} + e^- \rightarrow ZnTTP^{5-} \qquad (2)$$

occurs at a potential of –1.16 V [13]. Thus, the difference between the oxidation and reduction potentials are 0.87-(-1.16)V = 2.03 V. This difference correlates very well with the 2.05 eV energy of the S_1 state. The transient absorption spectra of both oxidised and reduced porphyrins show great similarities to the

observed spectra of the excited states. Thus, it has been suggested that the oxidation and the reduction reactions of regular porphyrins involve oxidation and reduction of the porphyrin ring. [18]

Excited state redox potentials can be calculated according to:

$$E^0_{P*/P+} = E^0_{P/P+} - E_{00} \quad (3)$$

and

$$E^0_{P*/P-} = E^0_{P/P-} + E_{00} \quad (4)$$

where E_{00} is the energy difference between the excited state and the ground state, in eV. (Note that eq. 4 in its form can be used only when the energy is treated in eV, and the E_{00} value should be considered as divided by a unitary charge). This can be calculated from the absorption and fluorescence spectra, where E_{00} is taken as the average energy of the 0-0 transitions of the absorption and fluorescence, respectively. For the E_{00} energy of the triplet, no absorption spectra is available, and the E_{00} energy was taken from the blue edge of the low temperature phosporescence. The excited state is both a stronger reductant and a stronger oxidant than the ground state molecule. In ZnTPPS, the E_{00} energy of the S_2 state is 2.9 eV and the S_1 E_{00} energy is 2.0 eV. Thus for the excited states, the oxidation and reduction occurs at –2.1V and 1.74 V for S_2, and –1.2V and 0.84 V for the S_1 state.

Hence, redox reactions that are endoergonic in the ground state can be exoergonic in the excited state. Further, a redox reaction that is endoergonic in the S_1 state can be exoergonic in the S_2 state. Hence, photoinduced electron transfer between an excited porphyrin and an electron acceptor will have different free energy difference depending on the reactive state of the porphyrin. This effect have been utilised in electron transfer reactions ion pairs of ZnTPPS and methyl viologen [**I**], and in a ZnTTP linked to a $Ru(bpy)_3^{2+}$ complex,[**II,V**].

3. Experimental methods.

This chapter descibes the different experimental techniques used in my work, especially the instrumentation in femtosecond experiments. The femtosecond experiments are based on the transient absorption technique, and in principle the methods in the femtosecond and in the nanosecond experiments are the same. Therefore, I will begin by describing the general features of the transient absorption experiment.

3.1. Transient absorption.

The transient absorption experiments involves irradiation of the sample with an excitation light pulse, followed by an analysing pulse.
The absorption of the sample prior to the excitation pulse is defined by:

$$Abs = -lg\ (I_o/I_{ref}) \qquad (5)$$

where I_o, I_{ref} is the intensity of the analysing light passing through two the sample and a reference solution respectively. When sample is irradiated with an excitation pulse in the same part of the sample as the analysing pulse, the absorption is given by:

$$Abs = -lg\ (I/I_{ref}) \qquad (6)$$

The difference between the absorption of the sample with and without illuminating with the excitation pulse is then:

$$\Delta Abs = -lg\ (I/I_{ref})-(-lg(I_o/I_{ref}))= lg\ (I_o/I) \qquad (7)$$

Thus, in order to measure the absorption of the excited state and the ground state, a reference light through the solvent is needed, while the difference absorption between the ground state and the excited state can be measured without a reference light.

Figure 3.1, show a transient absorption experiment in a tentative system. First, the absorption of the sample is measured without the excitation beam. Then, the sample is excited with a short light pulse.

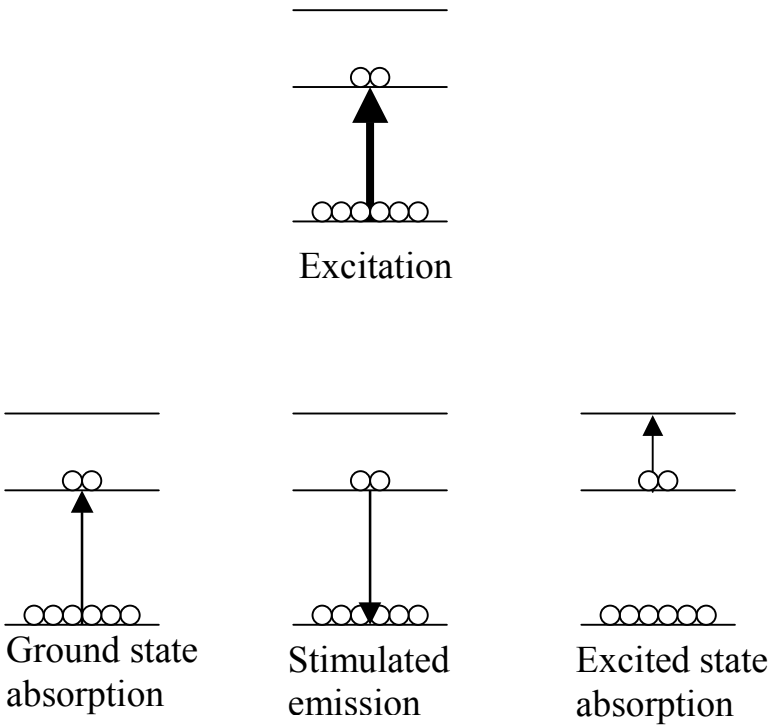

Figure 3.1

A fraction of the systems in the sample will interact with the excitation pulse, creating transitions between the S_0 and S_1 states. The probability of transition between the S_0 and S_1 states are proportional to the Einstein coefficients for optical transitions, which are equal in both directions. Thus, stimulated emission is as probable as absorption. If a probe light of the same frequency as the excitation light passes through the sample, the attenuation be less than in a non-excited sample, due to stimulated transitions from S_1 to S_0 and by a smaller number of systems in the S_0 state. The absorption difference of the sample prior to and after excitation will be less than zero (a bleach). However, if the probe light is of a frequency that corresponds to a transition from the S_1 to a higher excited state S_2, the attenuation of the probe light will increase. In summary, the net observed difference absorption can be written as

$$\Delta Abs = ESA-GSB-SE-E \quad (8)$$

where ESA is excited state absorption, GSB is ground state bleaching, SE and E is stimulated and natural emission.

3.2 The laser instrumentation

The fundamental laser in the system is a passively mode locked Ti saphire laser (MIRA^{TM}, Coherent Laser Systems). For a Ti saphire laser medium, the optimum laser wavelength is 800 nm, but the laser may operate in the wavelength range 700 to 900 nm. In figure 2.2, a schematic picture of the experimental setup is presented. The generation of ~80 fs, 76 MHz laser pulses are made by passively modelocking in the MIRA^{TM} cavity. The passive mode locking is achieved by utilising the Kerr lens effect in the Ti-saphire crystal, together with a variable slit. Although the pulses are not transform limited, the laser pulses obtained have normally a spectral bandwith of ~12 nm, or ~25 meV. The pulse intensity from the MIRA^{TM} is about 10 nJ, and in order to make a pump probe experiment, the pulses are amplified by two different laser systems: either by a Q switched 200 kHz Ti saphire laser connected to an optical parametric amplifier, or by a 1 KHz Q switched Ti saphire laser also connected to an optical parametric amplifier. In both systems, the 80 fs pulses of the MIRA is stretched by the use of a grating and a mirror, then seeded into the cavity together with a ns Q switched pulse. After amplification, the pulses are sent through the stretcher in the opposite direction, resulting in re-compressed pulses approximately 50% longer (~120 fs) and with ~400 resp. ~80 000 times higher intensities.

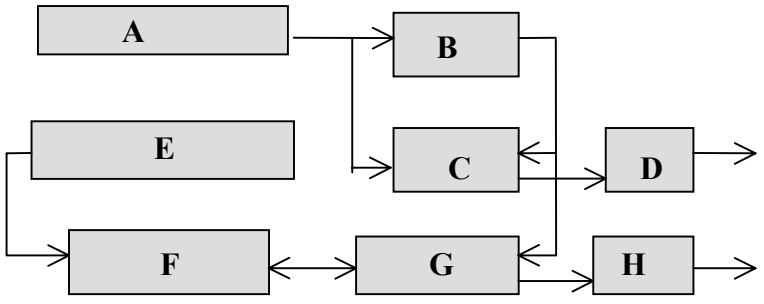

Figure 3.2 Laser experimental setup. *A*: Ar ion CW laser. *B*: Ti-saphire fundamental laser, (MIRA^{TM}), *C*: Ti-saphire amplifier laser (RegA^{TM}), *D*: Optical parametric amplifier (OPA^{TM}) *E*: Nd-YLF Q switched laser, *F*: Ti saphire amplifier laser, *G*: pulse stretcher/compressor, *H*: optical parametric amplifier (TOPAS^{TM})

3.3 Kinetic measurements

The principle of the pump-probe experiment is shown in figure 3.3. The 120 fs, 800 nm, 1 kHz output from the amplifier is split into two beams (70:30). The more intense fraction passes through the optical parametric amplifier (OPA), and wavelengths in the region 500-600 nm is obtained. The output of the OPA

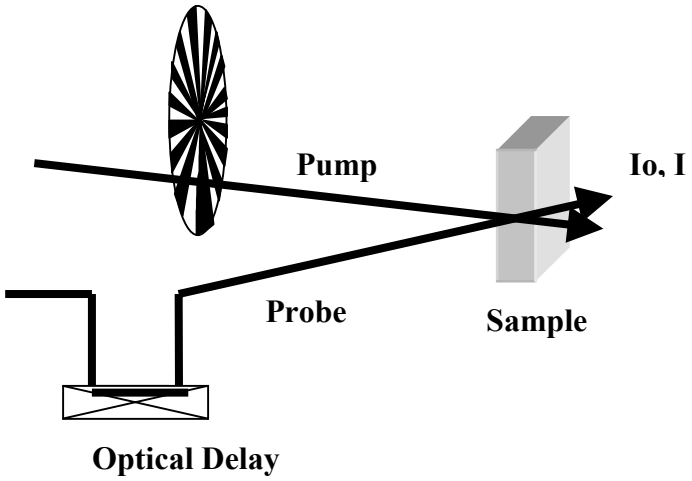

Figure 3.3 The principle of pump and probe.

passes through a chopper, operated at about 75 Hz. The excitation pulses are focused approximately 2 cm behind the sample by a 10 cm lens. The remaining 30% of the 800 nm output is softly focused into a 3 mm saphire window, to generate a white light continuum (WL). The WL is delayed by an optical delay line, and focused into the sample in the same volume as the pump pulses.
By the optical delay line, the distanced travelled by the WL probe light will be varied, while the distance travelled by the pump light is constant. Thereby, by calibration of the speed of light, the distance difference can be translated into time units. The optical delay line is moved by a step motor, controlled by a software (Labview^{TM}).

For transient absorption kinetic traces, the probe light passes through a monochromator, and on to a photomultiplier tube. The response from the photomultiper passes on to a lock-in amplifier (LIA). Figure 3.4 shows the principle of signal detection by the LIA technique. The change in the absorption varies with the chopping frequency of the pump pulses. The LIA detects only variations in the photomultiplier signal that matches the chopping frequency.

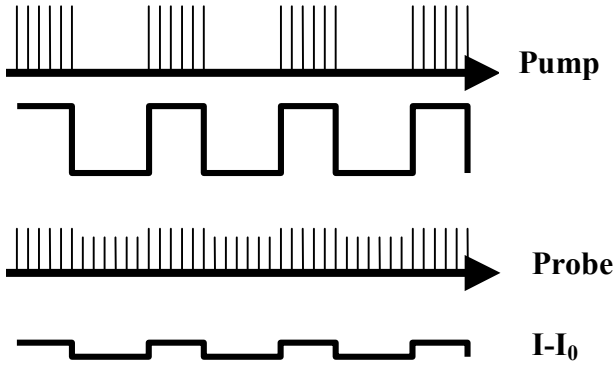

Figure 3.4 The signal from the LIA.

The LIA signal is given as $(I-I_0)$, whereas the ΔAbs is $-\lg(I/I_0)$. Thus, the magnitude of the observed LIA signal is dependent of the amount of white light detected, while the ΔAbs is independent of the magnitude of the white light intensity. This is a clear disadvantage of the LIA technique for the transient absorption. However, in many cases, the main interest is to follow the time evolution of a transient absorption signal. It can easily be shown that when the ΔAbs is small, the change of LIA signal per time unit can be approximated with the change of ΔAbs per time unit. Thus, the LIA signal can be used to follow the build up and the decay of a transient absorption, and thereby allow for kinetic analysis, while the magnitude of the transient absorption is not obtained. In the kinetic traces presented in papers **I-V**, the LIA signal has been used to monitor the kinetics. The ΔAbs are therefore given as arbitrary units, and the maximum ΔAbs is normalised to 1.

3.4 Transient absorption spectra.

Transient absorption spectra were obtained with a CCD. The WL is split into its wavelength components by a spectrograph, and the intensity is measured with and without excitation pulses. Difference absorption at each wavelength is calculated according to eq 7.

Due to the wavelength dependency of the refractive index, pulses of different wavelengths will travel with different speed through the optical delay line. Thus, the time delay between the pump pulses and the probe pulses will be depending

on the wavelength of the probe light that is monitored. The effect is referred to a group velocity dispersion, or chirp.
In figure 3.5 the measured time-zero at different wavelengths of the white light probe is shown. The figure shows that for the wavelength region 400 to 600 nm, there is a >3 ps difference between the time-zeros. In order to obtain transient absorption spectra at time delays shorter than about 10 ps, the spectra must be

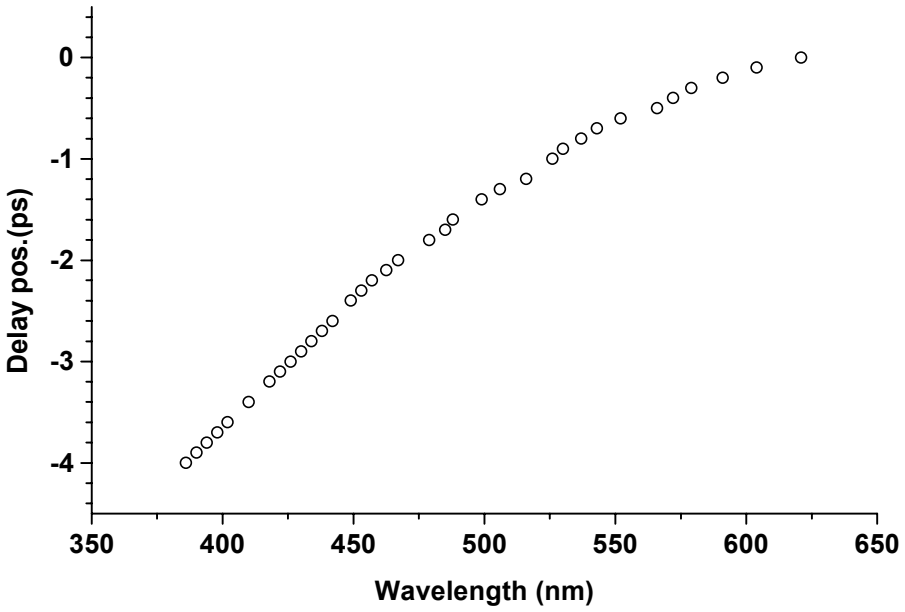

Figure 3.5 The measured time-zero at different wavelength of the white light continuum.

corrected. The observed chirp is a result of the GVD introduced by all the components between the place of white light generation and the overlap region in the sample. These components are reflecting mirrors, transparent lenses, the sample(cuvette and solvent) and also the air. However, for normal coated mirrors, the main GVD effect arises from the transparent optics. Thus, though in principle the chirp could be calculated if the refractive index in known for all the materials, the number of different components present are likely to introduce errors in the calculation. A more direct way to tackle the problem of GVD is to measure the pump- probe time zero at different wavelengths. Several methods are possible, including the use of a nonlinear crystal to measure the frequency mixing of the pump and the probe. This approach has the disadvantage of introducing optical (and chirp active) materials other than the ones used in the

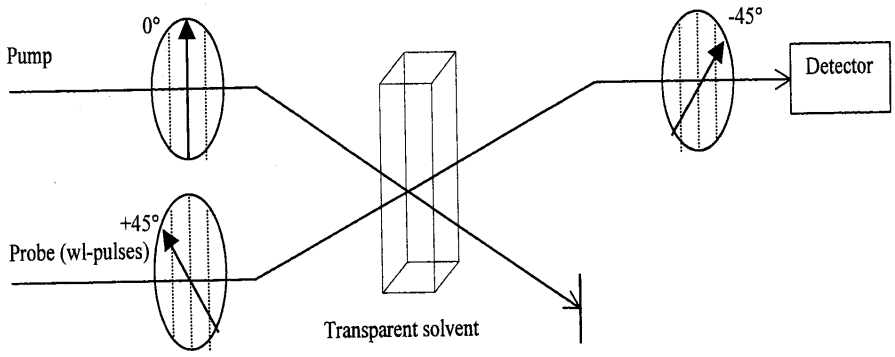

Figure 3.6 The principle of Kerr response for determination of I.R.F. and G.V.D. The circles represent polarising filters.

actual experiment. The nonlinear crystal itself might result in a chirp, which is different from the sample cell. Figure 3.6 show the method used in [**I**] which is based on the instantaneous electronic Kerr effect in solutions [30]. The Kerr response can be measured either as a time correlated response at a single wavelength, or as a spectral response at a single time delay. The main advantage of this method is that it allows for measuring the chirp in the same experimental setup as the actual pump-probe experiment is made, including the solvent of the cell. The peak of the Kerr curve is taken as being the time zero, and if one assumes that the pump and probe pulses are symmetrical, the instrumental response function can be obtained by fitting the risetime of the Kerr curve to a gaussian or secular hyperbolic function.

Once the chirp is characterised, transient spectra taken at small time delays can be corrected. In figure 2.4, the transient absorption spectra taken at early times were made by generating approximately 60 transient absorption spectra at different optical delay positions within the first 3 ps. A spectra at a certain delay time was then made by identifying the wavelength corresponding to that particular time in each spectra. The spectral resolution in this method is therefore dependent of the number of delay positions used, and in figure 2.4 the spectral resolution was 5 nm.

4. Electron Transfer.

4.1 Introduction

This section contains a basic description of the theory of electron electron transfer reactions. Since the theoretical work in this field is extensive, I will in this chapter only describe the basic features, and highlight the part of the theory most relevant for the work presented in papers **I-V**.

A molecular electron transfer reaction involves an oxidation of a donor (D) molecule and reduction of an acceptor molecule (A). If the donor and acceptor are freely diffusing in a solvent, then prior to electron transfer a bimolecular diffusion creates an encounter complex. In the encounter complex, electron transfer reaction occurs at a certain distance and arrangement. The encounter complex can either be in close contact, or in a solvent separated configuration, and electron transfer may occur at a distribution of different donor – acceptor configurations. The observed kinetics in such bimolecular reactions is a combination of the diffusion processes and the electron transfer reaction. If the donor and acceptor are attached to each other, no diffusion processes are needed prior to electron transfer, and unimolecular electron transfer reaction kinetic is observed. The theory describing electron transfer processes was developed from the transition state theory (TST) by Marcus [31-34] and has been further developed by others.[34-41]

4.2 Electron transfer in classical theory.

According to the classical transition state theory the electron transfer rate constant is given by:

$$k_{ET} = \kappa_{el} \upsilon_n \exp\left[\frac{-\ddot{A}G^{\#}}{k_B T}\right] \qquad (9)$$

where κ_{el} is the electronic transmission coefficient, ν_n is the nuclear frequency through the transition state, $\Delta G^{\#}$ is the Gibbs free energy of activation and k_B is the Boltzmann constant. The potential energy surfaces of the reactant and product states can be described as free energy surfaces, and electron transfer occurs at the crossing of the reactant and product surfaces. The amount of free energy required to bring the reactant to the crossing point is the free energy of activation, $\Delta G^{\#}$. If the free energy of the reactants and products are described as harmonic parabolas, with equal force constants, then according to Marcus the free energy of activation is:

$$\Delta G^{\#} = \frac{(\Delta G_0 + \lambda)^2}{4\lambda} \qquad (10)$$

And equation 9 is written as:

$$k_{ET} = \kappa_{el} \upsilon_n \exp\left[\frac{-(\ddot{A}\, G_0 + \lambda)^2}{4\lambda k_B T}\right] \qquad (11)$$

where λ is the reorganisation energy, defined as the change in free energy if the reactant state were to distort to the equilibrium configuration of the product state, without the transfer of an electron.

Figure 4.1 show the free energy curves for the reactants and products where the free energy difference between the products and reactants is varied. As ΔG^0 becomes more negative, $\Delta G^{\#}$ decreases, until $\Delta G^0 = -\lambda$, where $\Delta G^{\#} = 0$. A further decrease of ΔG^0 will cause $\Delta G^{\#}$ to increase again, and the reaction is said to occur in the Marcus Inverted Region (M.I.R.). Thus, in the M.I.R, as the driving force increases, electron transfer is slowed down. The first experimental observation of M.I.R was in frozen media, and later in solvent[42-44]. Since then, M.I.R behaviour has been established in a number of studies [45]. The original Marcus theory predicted a rapid decrease of the electron transfer rate in the M.I.R. Experimental data have shown that the decrease of the rate constants with the driving force is smaller than the original theory suggests. The rate constant has been found decrease exponentially with the driving force (energy gap law [40]). In the M.I.R., nuclear tunnelling between the reactant and product state is expected to be more important than in the normal region, and if tunnelling is added to the electron transfer theory, the difference between observed and expected rates becomes smaller. However, there have also been studies where the expected M.I.R behaviour was absent [46]. In bimolecular electron transfer, and in linked donor acceptor systems with flexible links, the electron transfer reaction may occur at different donor-acceptor distances, which will affect both the free energy driving force and the reorganisation energy. M.I.R behaviour is thus normally seen only in systems where the donor and acceptor is connected by rigid links with well defined donor – acceptor distances.

Note however, that a well-defined donor – acceptor geometry can be obtained also in systems without a rigid, covalent link. For example, a protein matrix,

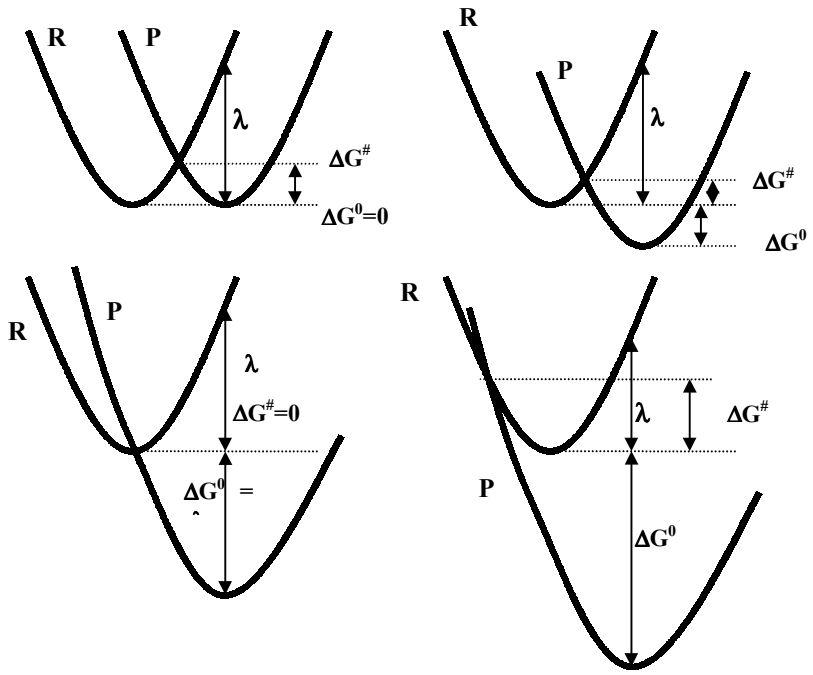

Figure 4.1
Electron transfer reactions with different values of the thermodynamic driving force. R,P denotes reactant and product states.

where the donor and acceptor are held in position by electrostatic effects, hydrogen bonds or covalent bonds, will certainly provide for a well defined geometry.

4.3 The Reorganisation Energy

The reorganisation energy can be divided into the inner and outer reorganisation. The inner reorganisation is the intramolecular, or inner shell, contribution to the total reorganisation energy. This is the sum of all the molecular vibrational and rotational movements. The inner reorganisation energy can be calculated as: [34]

$$\lambda_{in} = \frac{1}{2}\sum_i \overline{f_i}(r_R^{eq} - r_P^{eq})^2 \qquad (12)$$

where f is the reduced force constant of the i th vibration, and $r_{R,P}^{eq}$ is the equilibrium bond lengths of the reactant and product states. The calculation of

the inner reorganisation energy has been done in some studies. Normally, for rigid molecules and in polar solvents, the contribution of λ_i to the total λ is minor, with typicall values of 0.2 eV for λ_i [47, 48].

The outer reorganisation energy is the solvent, or outer sphere, contribution to the reorganisation energy. If one assumes a solvent that can be described as a dielectric continuum, λ_{out} can be calculated in the simple case of spherical reactants:

$$\lambda_{out} = \frac{(\Delta e)^2}{4\pi\varepsilon_0}\left[\frac{1}{2a_D} + \frac{1}{2a_A} - \frac{1}{r_{DA}}\right]\left[\frac{1}{\varepsilon_{op}} - \frac{1}{\varepsilon_s}\right] \qquad (13)$$

where Δe is the charge involved (usually 1 electron), ε_0 is the vacuum permittivity, ε_{op} and ε_s is the optical and static dielectric constants, $a_{D,A}$ the donor and acceptor radii and r_{DA} is the donor – acceptor center to center distance. The outer reorganisation energy is thus larger for a polar solvent than for a non polar solvent, and increases with decreasing donor/acceptor radii and donor- acceptor distances. In polar solvents, λ_{out} is proportional to $1/\varepsilon_{op}$.

4.4 Aspects of M.I.R. in photosynthetic reactions.

In a photosynthetic system consisting of several electron transfer steps, one wishes to suppress the unwanted back electron transfer reactions in favour of the next forward reactions. i.e. the ratio between the forward and back electron transfer reactions should be as high as possible. The energy obtained in the end of the reaction sequence should be as high as possible. Thus, each forward reaction step should involve a small reaction free energy. Hence, the competing charge recombination reaction will have a larger driving force than the next forward reaction. However, if the forward reaction occurs with near zero activation energy, the back reaction will be in the M.I.R. region. Thus, in the design of photosynthetic systems, it is desirable to allow the forward electron transfer steps to occur with small free energy of activation. Further, in order for the reaction to occur with minimum activation energy, the free energy should equal the reorganisation energy. For electron transfer between donor and acceptor with moderately high electronic coupling, the electron transfer will occur at rates in the ps and fs time scales.

4.5 Electron transfer with quantum mechanical aspects

In a quantum mechanical description of non adiabatic electron transfer, the rate constant can be written as [34]

$$k = \frac{2\pi}{\hbar} H_{AB}^{2} (FCWD) \qquad (14)$$

where H_{AB} is the electronic matrix element describing the electronic coupling between the reactant and product states, and FCWD is the Frank Condon weighted density of states, which can be described as a Boltzman weighted sum of overlap integrals of the solvational and vibrational wavefunctions. One treatment of the FCWD factor is to separate out the solvent contribution, and treat the solvent as classical, and the internal vibrational wavefunctions as harmonic oscillators. Then, in the limit where the energy corresponding to each of the vibrational frequencies is considerably less than the thermal energy, ($h\nu_i << k_B T$), eq. 14 can be approximated as:[34]

$$k = \frac{2\pi}{\hbar} H_{AB}^{2} \frac{1}{(4\pi\lambda k_B T)^{1/2}} \exp\left[-\frac{(\Delta G^0 + \lambda)^2}{4\lambda k_B T} \right] \qquad (15)$$

which is called the high temperature rate expression. When vibrations of higher frequencies are coupled to the electron transfer, eq. 15 no longer holds. If the solvent is still considered as a bath of harmonic oscillators with low frequencies, one average high intramolecular frequency can be introduced [49], leading to:

$$k = \frac{2\pi}{\hbar} H_{AB}^{2} \frac{1}{(4\pi\lambda_0 k_B T)^{1/2}} \sum_{w=0}^{\infty} \exp^{(-S)} \frac{S^w}{w!} \exp\left[\frac{-(\lambda_0 + w\hbar\nu + \Delta G^0}{4\lambda_0 k_B T} \right]$$

$$S = \frac{\lambda_i}{\hbar\nu} \qquad (16, 17)$$

Thus, with equation 15 and 16, the rate constant of an electron transfer reaction can be predicted, provided that the different parameters are known, or can be properly evaluated from experimental results.

4.6 The electronic coupling, H_{AB}

Depending on the magnitude of the electronic coupling between the donor and acceptor, the electron transfer reaction can be classified as adiabatic or non adiabatic. For a non adiabatic reaction $\kappa_{el} << 1$ in equation 9, while in the limit of adiabatic electron transfer $\kappa_{el} \approx 1$. In the non adiabatic limit, the probability of crossing over from the reactant state to the product state is relatively small, and the crossing is considered as a sudden event [39]. In the adiabatic reaction, the reactant and product free energy curves are split to a lower and an upper curve, and the reaction is thought to proceed along the lower curve, as shown in figure 4.2.

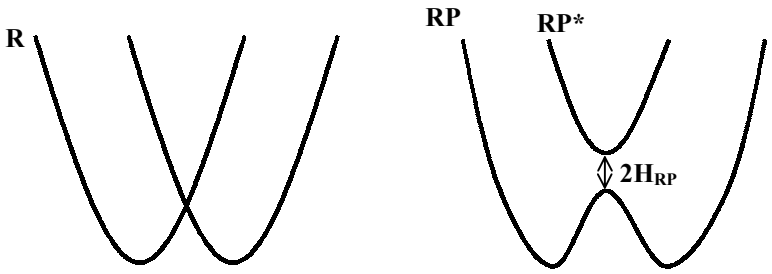

Figure 4.2. Non adiabatic (left) and adiabatic (right) electron transfer. In the non adiabatic reaction, the reactant and product are described by two curves, while in the adiabatic reaction the reactant and product form a lower and an upper free energy surface. At the transition state, the energy separation are $2 \times H_{RP}$

Equations 15,16 gives the rate constant for a non adiabatic electron transfer. Modifications to include reactions in the adiabatic region have been suggested by Bixon/Jortner [50, 51]:

$$k_{ET} = \frac{k_{NA}}{1 + \kappa_A} \qquad (18)$$

where k_{NA} is the rate constant in the non adiabatic limit (eq. 15), and κ_A is the adiabatic parameter:

$$\kappa_A = \frac{4\pi H_{AB}^2 \tau_l}{\hbar \lambda_o} \qquad (19)$$

τ_l is the longitudinal relaxation time of the solvent. If the adiabatic factor is <<1, equation 18 is corresponds to equation 15. However, with increasing electronic coupling, the adiabatic factor increases, and in the limit where κ_A>>1, equation 11 becomes:

$$k_{ET} = (\tau_l)^{-1} (\lambda_o / 16\pi kT)^{1/2} \exp(-\frac{\Delta G^{\#}}{kT}) \qquad (20)$$

Thus, the rate constant will be proportional to the solvent relaxation time. The rate will depend of the rate of which the solvent will rearrange to solvate the change of charges of the reactant and product. According to eqs. 18,19 the criteria for when the reaction occurs in the non adiabatic and the adiabatic limits depends not only on the electronic coupling, but rather on the relation between the solvent properties and the electronic coupling.

H_{AB} is dependent on the donor and acceptor distance. This can be understood by the fact that the electronic wavefunctions in the donor and acceptor molecules display a distance dependence, and hence the overlap should be distance dependent. At large distance from the nucleus, the electronic wavefunctions decay exponentially with distance, and the electronic coupling is thus expected to depend exponentially on the distance. This has been found experimentally [43, 53-57], and the distance dependency can be written as:

$$k = k_0 \exp(-\beta(r-r_0)) \qquad (21)$$

r_0 is the donor-acceptor centre to centre distance at optimum electronic coupling, and can be calculated as the sum of the donor and acceptor radius. The value of β varies, depending on the nature of the intervening medium between the donor and acceptor. Through-solvent electron transfer becomes rather slow already at moderate donor acceptor distances. In order for electron transfer to occur fast at appreciable distances, the electronic coupling between the donor and acceptor should be increased by interaction of intervening media other than pure solvent.

4.7 Bridge mediated electron transfer

The donor – acceptor electronic coupling can be enhanced by the presence of an intervening medium. In this case, the total donor acceptor coupling can be divided into the coupling of the donor with the different link states, the link-link coupling and the acceptor- link interactions. The intervening medium can be solvent molecules, residues in a protein backbone, direct covalent link, hydrogen bonds or coordination bond or it can be a combination of several of the above mentioned. In a complex structure, like in a protein, there may exist several possible electron transfer pathways, with different donor- acceptor couplings. [58-64]

The bridge mediated electron transfer mechanism can be divided into two categories; superexchange and sequential electron transfer. In a superexchange mechanism [65], the energy of the link is higher than the donor energy, and electron transfer from the donor to the link is energetically unfavourable. The link takes part in promoting electron transfer, but the electron is never resident on the link, instead the electron transfer may occur through a virtual state. On the other hand, if the energy of the link is closer to or even between that of the donor and the acceptor, electron transfer occurs by a stepwise mechanism. The intermediate state, with a reduced link might be observed, but if the secondary electron transfer step is much faster than the initial step, the intermediate state becomes practically impossible to detect. In paper [IV], both a superexchange mechanism and a proposed sequential mechanism is proposed.

In figures 3 and 4 the principle of the superexchange and sequential mechanisms is shown schematically. Note that in the picture, the link is represented by a single state. In reality, one has to consider all the possible states that might be involved in promoting the donor – acceptor coupling. In the superexchange mechanism, H_{DA} can be expressed by: [39,40]

$$H_{DA} = \sum V(Dl_n)V(Al_n)/\Delta E_n \qquad (22)$$

where ΔE_n is the free energy difference between the donor and the n:th link, and V is the electronic coupling of the donor resp. acceptor with the n:th link.

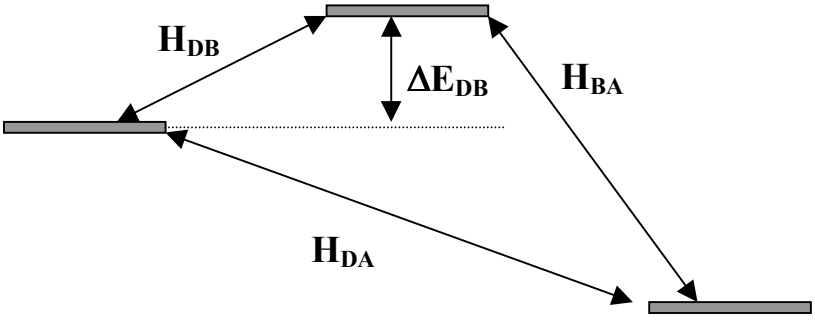

Figure 4.3 Superexchange mechanism. The bridge is represented by a single state, that is higher in energy than the donor state.

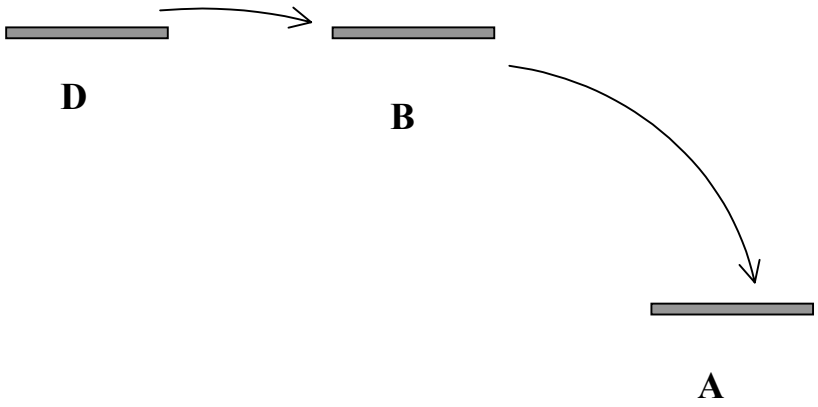

Figure 4.4 Sequential mechanism. The bridge is represented by a single state, with energy low enough so that population of the bridge may be thermally promoted.

4.8 Experimental determination of parameters

The free energy difference, ΔG^0, can be obtained by electrochemical measurements:

$$\Delta G^0 = -nF\Delta E^0 + \Delta w \qquad (23)$$

where ΔE^0 is the difference between the redox potentials for the donor and acceptor molecules, and Δw compensates for that the measured redox potentials are for infinite donor-acceptor distance, while the donor acceptor distance in the reaction introduces Coulombic forces. This correction introduces a distance dependence of the reaction free energy. Hence, if the Coulomb forces are not negligible (at short distances and nonpolar solvents), the driving force calculated from the redox potentials should be corrected for.

From eq. 15, the temperature dependence of the observed rate constant can yield the total reorganisation energy, if the reorganisation energy is assumed to be temperature independent. The reorganisation energy of the solvent can be calculated, if one assumes a dielectric continuum, spherical donor and acceptor molecules with known radius and distance (see above), and hence the inner reorganisation energy can be obtained simply as $\lambda_i = \lambda_{tot} - \lambda_{out}$. If λ_i is known, the Huang-Rhys factor (S, eq 17) can be calculated, provided that one average high frequency mode can be assumed.

The electronic coupling, H_{AB} is the most difficult parameter to obtain experimentally. However, according to the theory by Hush [38], if a direct charge transfer (CT) band can be observed, H_{AB} can be calculated from the shape and intensity of the charge transfer band. Often, the intensity of the CT band is very low, making it difficult to measure in practice. Nevertheless, CT bands have been observed for several systems, for which H_{AB} could be evaluated.[66]

5. Reactions from higher excited states

5.1 Why study electron transfer from higher excited states?

As described in Chapter 2, regular metal porphyrins display a strong transition around 420 nm, denoted the Soret band. Upon absorption, the S_2 state of the porphyrin is populated. The energy difference between the S_1 and S_2 state is almost 1 eV. This large energy difference contributes to make the lifetime of the S_2 state relatively long, according to the energy gap law. Porphyrins have been used in a number of synthetic model systems for photosynthetic reactions [52, 67-85] and electron transfer has been demonstrated to occur on a sub-picosecond time scale [21,52,79-86]. These studies have all considered electron transfer reactions from the S_1 state. Despite the large number of porphyrin donor-acceptor systems studied, reports on reactions from the S_2 state are easily counted [I,II,V,21]. Recently, *energy* transfer from the S_2 state of a Zn-porphyrin linked to $Ru(bpy)_3^{2+}$ was reported. [78, 87]. With a lifetime of a few ps for the S_2 state, electron transfer reactions could occur prior to internal conversion to S_1, if the donor and acceptor are sufficiently strongly coupled.

A reaction from the higher excited S_2 state is interesting in several respects: For photosynthetic systems, the energy of S_2 is almost 1 eV higher than the corresponding S_1 state. Thus, photoinduced electron transfer can occur with electron acceptors that are more difficult to reduce than what is energetically possible with reactions from the S_1 state, and in principle, more energy can be harvested in each reaction. Further, small molecular "machines" have been constructed by several groups, where photoinduced electron or energy transfer is followed by molecular rearrangements [2]. Molecular switches have been constructed [5] and in [3,4] the formation and lifetime of products were controlled by excitation with two femtosecond laser pulses with a well defined separation in time. With reactions from the S_2 state, new reaction channels can be introduced, in competition with reactions from the S_1 state. In principle, molecular machines and switches with different responses depending on the excitation wavelength can be constructed. Figure 1.1 shows a tentative system, consisting of a Zn porphyrin connected to two different acceptors, A1 and A2, that have different redox potentials. Electron transfer from the S_1 state to A1 is exoergonic , and endoergonic to the A2 acceptor. From the S_2 state, electron transfer is exoergonic to both the A1 and A2 acceptors, but ideally the electron transfer to the A1 is in the M. I. R. and with a weaker coupling and thus slowed down compared to the reaction to A2.

In paper [I] very fast (<200 fs) electron transfer was seen from the S_2 state of $ZnTPPS^{4-}$ to complexed MV^{2+}. The electron transfer is one of the fastest observed in molecular systems. However, the reaction occurs also rapidly from the S_1 state [79, 88]. In order obtain selectivity of electron transfer the redox potential of the acceptor should be such that electron transfer from the S_1 state is endoergonic. In [II, V], the electron transfer reactions with a linked $Ru(bpy)_3^{2+}$ as acceptor was studied. The free energy of electron transfer from the S_1 is very small, and indeed a clear difference between the electron transfer rates from the S_2 state and the S_1 state was observed. Further, the rate of electron transfer from the S_2 state could be resolved. Also, the formation of a triplet (porphyrin) state from a charge transfer state was observed in the ZnTTP-L-$Ru(bpy)_3^{2+}$ dyad. Formation of a triplet from a radical pair has been reported [89].

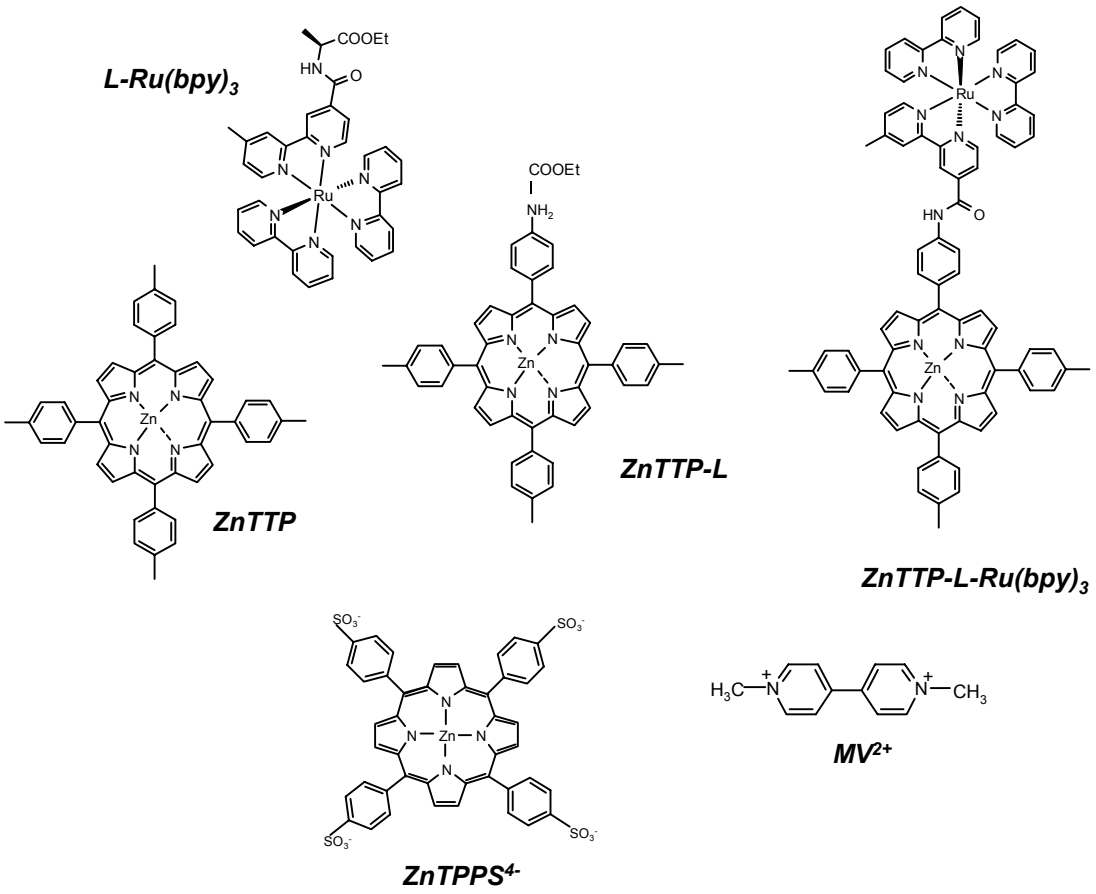

Figure 5.1
Structures of porphyrins and acceptors.

5.2 Molecules studied

In figure 5.1, the structures of the investigated molecules are presented. In [I], the S_2 lifetime of $ZnTPPS^{4-}$ and electron transfer reactions in the $ZnTPPS^{4-}$-MV^{2+} ion pair was studied. In [II, V], the S_2 lifetime in the ZnTTP-L and ZnTTP references, and electron transfer reactions upon selective excitation of the porphyrin S_2 and S_1 states of the ZnTTP-L-$Ru(bpy)_3^{2+}$ dyad was investigated.

5.3 Lifetime of the S_2 state in the Zn porphyrins

The lifetime of the S_2 state was measured for $ZnTPPS^{4-}$ (in water)[**I**], ZnTTP (in DMF)[**II**] and ZnTTP-L (in acetonitrile)[**V**] by transient absorption, and the results are presented in Table 4.1. In figure 2.4, the transient spectra of $ZnTPPS^{4-}$ at early times upon excitation are shown. In the Soret region, strong bleach is observed (not shown), while in the 440 to 550 nm region a broad transient absorption with a peak around 465 nm is seen. The spectrum at 10 ps corresponds to the transient absorption spectrum of the S_1 state of ZnTPP [18]. The spectra at early times in figure 2.4 show mainly the transient absorption features of the S_2 state. The lifetime of S_2 was measured at several probe wavelengths, and the internal S_2 to S_1 internal conversion could be monitored in the whole region 420-550 nm as an increase of the transient absorption. On the blue side of the Soret band, at 390 nm, the S_2 state displays stronger absorption than both the ground state and the S_1 state, and the S_2 to S_1 internal conversion is seen as a decay. At 435 nm, the transient absorption of the S_1 state is close to zero, while the S_2 state displays a bleaching. The nature of this bleaching is likely to be a combination of ground state bleaching and stimulated emission. Figure 2.5 shows the transient absorption signal (upon 424 nm excitation) at 435 nm and 390 nm for the $ZnTPPS^{4-}$,[**I**] and in figure 5.2 the corresponding 435 nm transient is shown for ZnTTP and ZnTTP-L-$Ru(bpy)_3$. [II] When $ZnTPPS^{4-}$ is probed in the Soret peak, at 420 nm, a strong initial bleach is seen to recover to half its original value, consistent with the presence of stimulated emission [I, fig.3]. Fluorescence up conversion studies by Gurzadian et. al. [23] of the S_2 lifetime has shown that the decay of the S_2 emission matches the rise time of the S_1 emission, indicating that internal vibrational relaxation within S_1 is considerably faster than the S_2 to S_1 relaxation. In [I], the measured lifetime of the S_2 state was independent of the probing wavelength. Thus, the decay of the stimulated emission from the S_2 state (at 420 nm) and the risetime of the transient absorption from the S_1 state (i.e. at 435 nm) matched very well. Hence, the observed 1.3 ps lifetime does not reflect internal vibrational relaxation within the S_1 state, but rather the decay of the S_2 state, which is also consistent with the findings of Gurzadian et. al.

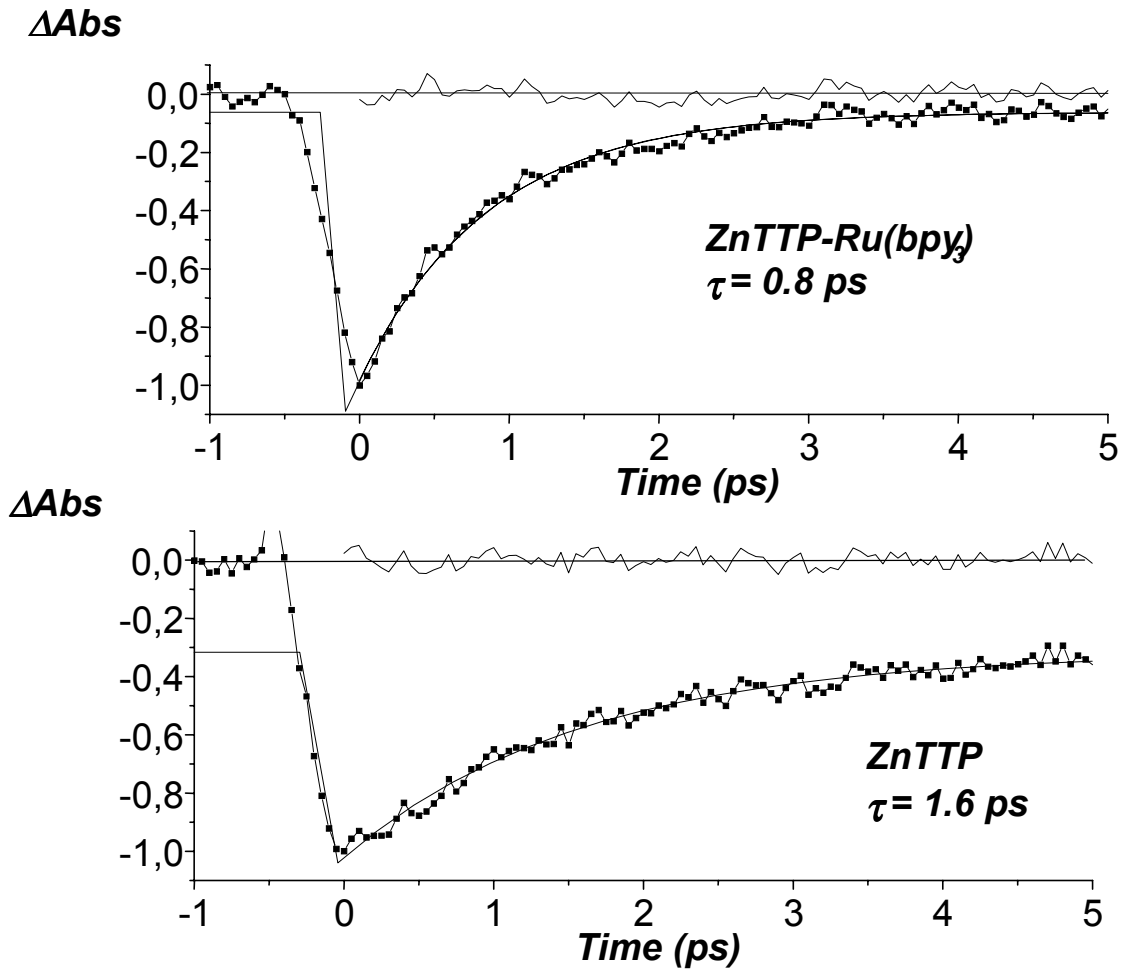

Figure 5.2 Transient absorption at 435 nm upon 414 nm excitation of ZnTTP (top) and ZnTTP-L-Ru(bpy)$_3^{2+}$. The lifetime of S_2 was obtained from the recovery of the bleach.

5.4 Electron transfer in the ZnTPPS^{4-}- MV^{2+} complex

When MV^{2+} was added to an aqueous solution of $ZnTPPS^{4-}$ with 2 mM phosphate buffer at pH 7, 1:1 complexes were formed. Figure 1, paper **I** shows the absorption changes in the Soret band of $ZnTPPS^{4-}$ upon titration with MV^{2+}. Isosbestic points were seen both in the Soret and Q bands, and the Soret band was shifted 7.5 nm. The steady state emission was studied, and the results could be successfully treated according to the Stern Vollmer procedure [90], which gave an association constant of 1×10^4 M^{-1}. The presence of isosbestic points, the Stern Vollmer behaviour and the Job plot performed by Logunov et. al. [79] strongly indicates the formation of 1:1 complexes between $ZnTPPS^{4-}$ and MV^{2+}.

Table 5.1

	Lifetime	Solvent
$ZnTPPS^{4-}$	**1.3 ps**	**water[a]**
ZnTTP	**1.6 ps**	**DMF**
ZnTTP-L	**2.3 ps**	**Acetonitrile**

a) 2 mM phosphate buffer, at pH 7.0

Upon reduction, the absorption spectra of methyl viologen changes dramatically in the visible region, with generation of a strong absorption centered at 396 nm, and a broad absorption peak around 600 nm, that extends into the NIR [91]. Electron transfer from $ZnTPPS^{4-}$ to MV^{2+} created the charge transfer state $ZnTPPS^{3-}$ - $MV^{+\cdot}$, and the reduced methyl viologen could be detected e.g. by the absorption changes in the 396 nm region. The complex was excited in the Soret band of $ZnTPPS^{4-}$, and probed at various wavelengths, and the formation and decay of the charge transfer products were studied [Fig. 5b and 6b in paper **I**]. The formation of the charge transfer products could not be resolved from the instrumental response of the pump and probe pulses, indicating an electron transfer constant larger than 5×10^{12} s^{-1}. The back electron transfer was monitored as the decay of the transient absorption, and the rate constant for the back electron transfer was found to be $1.3\times10^{12}s^{-1}$. The observed lifetime of the charge separated state was independent of the probing wavelength, and hence no vibrational relaxation was observed in the charge transfer state. The observed lifetimes in the $ZnTPPS^{4-}$ and the $ZnTPPS^{4-}$ - MV^{2+} complex are presented in figure 5.3

In the studies of the electron transfer upon S_1 excitaion [79,88], the rate of the back electron transfer was compared in a series of acceptor, and for $ZnTPPS^{4-}$ MV^{2+} it was found to occur in the Marcus inverted region (close to the maximum of the Marcus parabola) [79]. The rate of the forward electron transfer from the S_1 suggests that also this reaction occur with a near maximum rate. With a near activationless electron transfer from the S_1 state, one might expect the reaction from the S_2 state to occur in the M.I.R., since the energy of the S_2 state is almost 1 eV higher than the S_1 state. Thus the observation of <200 fs electron transfer deserves a comment.

For electron transfer in polar solvents, a solvent reorganisation energy of approxymately 1 eV is not unlikely, and Logunov et.al [79] obtained 1.3 eV. The free energy for the electron transfer reactions from the different states can be estimated from the redox potentials of the S_2 and S_1 states and the redox potential for the $MV^{2+/+}$ pair. For electron transfer from the S_1 and S_2 states, $\Delta G^0 = -0.8$ eV and $\Delta G^0 = -1.7$ eV, respectively (without correction of electrostatic interaction between the donor and acceptor). Thus, the reported fast electron transfer from the S_1 state is consistent with a small activation energy, while the S_2 reaction would occur in the M.I.R. The observation of fast electron transfer from the S_2 state can be explained if electron transfer proceeds via excited states of the product, with a $\Delta G^{\#} \approx 0$, followed by rapid internal relaxation. Indeed, the absorption spectrum of reduced methyl viologen [91] show the presence of low lying excited states.

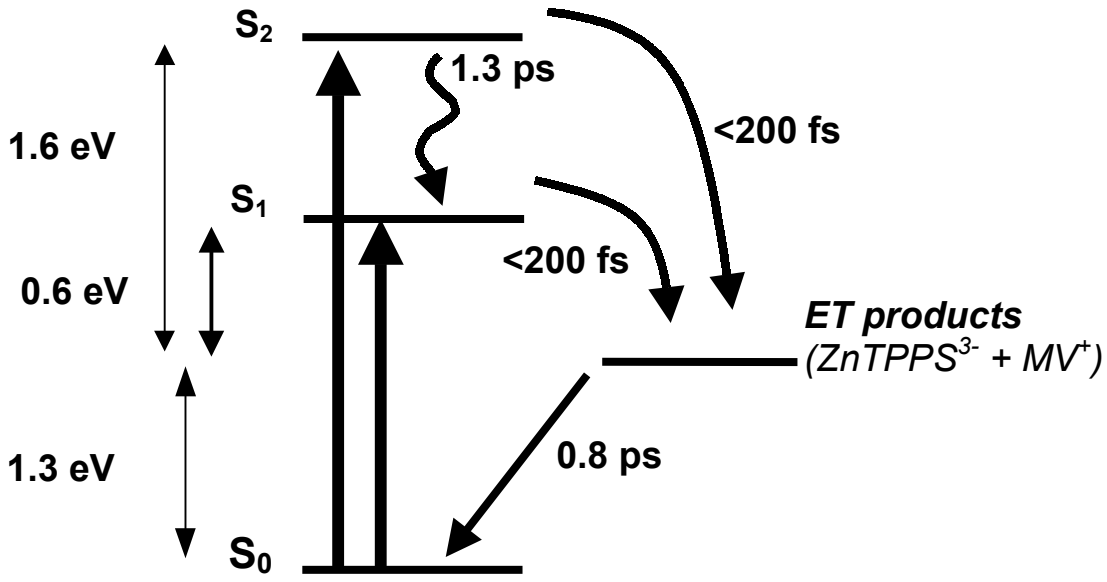

Figure 5.3 Internal conversion and electron transfer processes in the $ZnTPPS^{4-}$-MV^{2+} ion pair.

From the observation of a rate constant $>5\times10^{12}$ s^{-1}, and an estimated reorganisation energy of ≈1 eV, and the assumption that the reaction is activationless, the electronic coupling, H_{DA} can estimated to be >130 cm^{-1}. Thus, the forward electron transfer reaction is probably not purely non adiabatic, and solvent dynamics is expected to influence the rate of the observed electron transfer. In water, very short inertial relaxation times <100 fs has been reported [94], and an electron transfer within 200 fs is possible, also if the reaction is controlled by solvent dynamics.

5.5 Electron and energy transfer processes in the ZnTTP-L-Ru(bpy)$_3$ dyad.

The dyad was excited in the Soret and Q bands (414 nm and 560 nm) of the ZnTTP unit, and in the MLCT band (450 nm) of the $Ru(bpy)_3^{2+}$ unit. In paper [II] the observation of electron transfer from the S_2 state is reported, with a rate corresponding to a 50% quantum yield of charge transfer products, and in [V] the processes occuring upon the different selective excitations are further studied and clarified. In [78] energy transfer from the porphyrin S2 state was reported for a structurally similar dyad. In [87] the results in [I] and [78] were compared and commented. In [II], there were several indications that electron transfer, and not energy transfer is the main reason for the shortened lifetime of the S_2 state. However, some of the measurements done in [II] were repeated, and the results obtained indicated a need for further investigation. Paper [V] includes meaurements of the S2 lifetime of the dyad, and also with a reference porphyrin that are more structurally similar to the ZnTTP subunit in the dyad. Further, in [V], the reactions occuring upon excitation of the $Ru(bpy)_3^{2+}$ unit is investigated, as well as the processes occurring upon excitation to the S_1 state. The results in [V] further supports the conclusions in [II], that electron transfer takes place from the S2 state to $Ru(bpy)_3^{2+}$with a rate constant of 8×10^{11} s^{-1}. The observed rates of electron transfer from papers II and V are given in Table 5.2

In [**II**], the lifetime of the S_2 state was found to be reduced to 50% of that of the model ZnTTP, measured by transient absorption (figure 5.2). Steady state S_1 fluorescence quantum yield of the dyad was compared with the model ZnTTP. When the dyad was excited in the Q bands, the emission intensity was 13% of that for the ZnTTP, while Soret band excitation resulted in an S_1 fluerescence of 7% compared with ZnTTP. The steady state emission intensities show that the shorter S_2 lifetime observed in the dyad did not originate in an enhanced internal

S_2 to S_1 internal relaxation. Instead, a new reaction channel from the S_2 state exists in the dyad. In order to determine the nature (energy- or electron transfer) of the process responsible for the deactivation, transient spectra were recorded in the dyad. Figure 5.6 show the transient absorption recorded 10 ps after excitation of the dyad with 414 nm laser pulses. The spectrum was consistent with a combination of 50% S_1 state of ZnTTP[**I**,18] and 50 % oxidised $ZnTTP^+$ [**V**,18,27,95-97] and reduced $Ru(bpy)_3^+$ [98]. Electron transfer from the S_2 state occurs with a 50 % yield, and after 10 ps, the transient spectra consists of 50% from the S_1 state, and 50 % of charge transfer products. The transient absorption of both excited and reduced $Ru(bpy)_3^{2+}$ show a bleach in the region between 400 and 500 nm, and the effect of this bleach can been seen in the transient spectra in the 450 to 500 region. The spectral structures indicated by the arrows were interpretated as originating from the reduced $Ru(bpy)_3^+$ unit in paper [II].

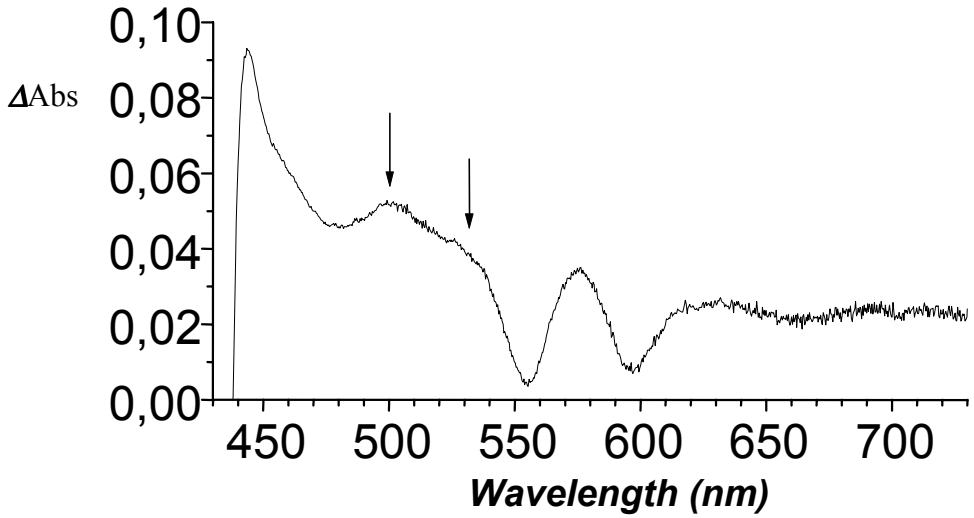

Figure 5.5
Transient absorption spectrum of the ZnTTP-L-$Ru(bpy)_3^{2+}$ dyad generated at a time delay of 10 ps after excitation in the Soret band. From [**II**]

Table 5.2 Electron transfer rate constants

	S_2 k_{ET} (s^{-1})	S_1 k_{ET} (s^{-1})
$ZnTPPS^{4-}$-MV^{2+}	**$>6\times10^{12}$**	**$>6\times10^{12}$** [79]
ZnTTP-L-$Ru(bpy)_3$ (DMF)	**6.2×10^{11}**	**9.5×10^{10}**
ZnTTP-L-$Ru(bpy)_3$ (acetonitrile)	**7.5×10^{11}**	**9.5×10^{10}**

In [II], upon excitation in the MLCT band at 450 nm of the $Ru(bpy)_3^{2+}$ unit in the dyad, a small amout of emission from $*Ru(bpy)_3^{2+}$ excited state was detected. In paper [II], we concluded that although the $*Ru(bpy)_3$ emission is strongly quenched by energy transfer to form the ^{3}ZnTTP triplet, we would be able to detect a small amount of emission if the deactivation channel from S_2 was energy transfer. However, in a further study of the dyad, we noticed the presence of a small fraction of dissociated dyad. Thus, monomeric $Ru(bpy)_3^{2+}$ or $Ru(bpy)_3^{2+}$-L is most likely to be responsible for the observed emission upon 450 nm excitation. This was easily confirmed by purging the solution with nitrogen gas, to remove the quenching by oxygen on a longer time scale. The steady state emission increased in intensity, as expected for dissociated $Ru(bpy)_3^{2+}$ units.

Therefore, in order to further establish what mechanism is responsible for the deactivation of the S_2 state in the dyad, the transient absorption studies in [V] were made. These are presented in paper [V]. Furthermore, the solvent used in paper [V] is acetonitrile, while in paper [II] the study were made in DMF. In [V], we used the ZnTTP-L as reference for the S_2 lifetime. The poor solubility of this compound in DMF motivated the change of solvent. In figure 5.7, the different processes observed upon excitation of the different states in the dyad is given. One of the most important findings in [V] is the observation of a development of new transient features upon the charge transfer reaction, which had a long lifetime, and displayed spectral features identical to the ZnTTP triplet state.

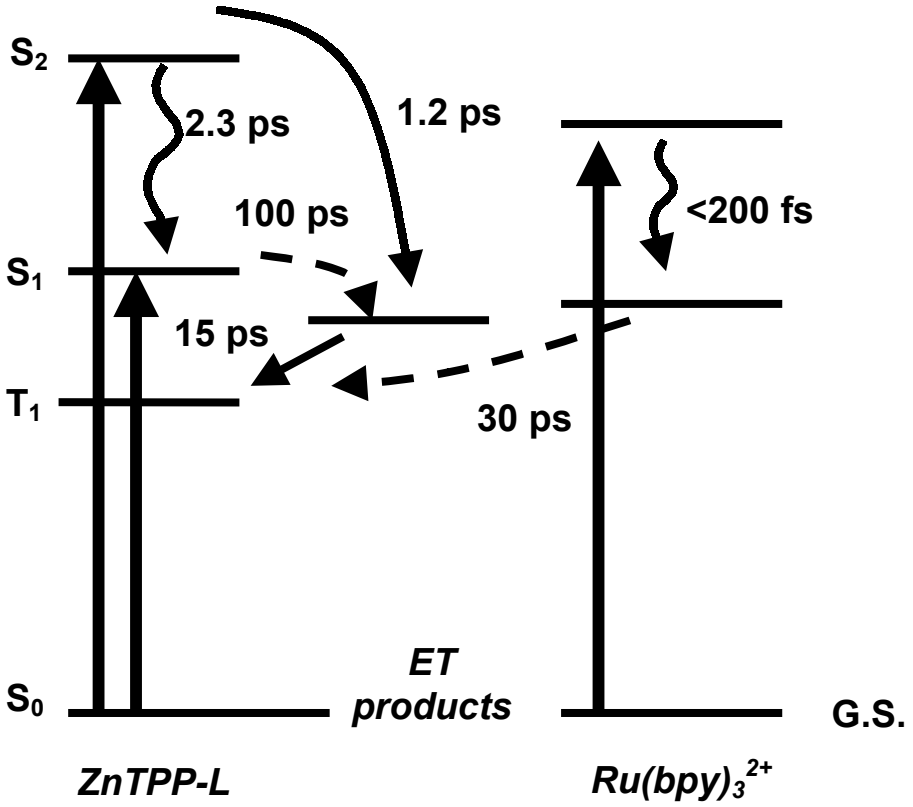

Figure 5.7 Internal relaxation, energy – and electron transfer processes in the ZnTTP-L-Ru(bpy)$_3$ dyad.

6. Electron- and energy transfer mechanisms in [2]-rotaxanes.

6.1 [2]-rotaxanes as model systems in electron transfer reactions

Rotaxanes in general have the topology of a ring threaded on a rod with stoppers to prevent dissociation. The [2]- rotaxanes studied in papers [III, IV] consist of two Zn(II) porphyrin (ZnP) donors attached as stoppers on a rod (figure 6.1, 6.2). A macrocycle ring with a Au(III) porphyrin (AuP^+) acceptor is threaded on the rod. The two phenanthrolines, one on the macrocycle and one on the rod, can coordinate metal cations. With no coordinated metal (**Zn_2Au^+**), the rod and the ring are held together only by mechanical bonds, while binding of a metal cation to the phenanthrolines connects the rod and the ring by coordination bonds (**$Zn_2Cu^+Au^+$** and **$Zn_2Ag^+Au^+$**). In **Zn_2Cu^+**, no Au(III) porphyrin is attached to the macrocycle.

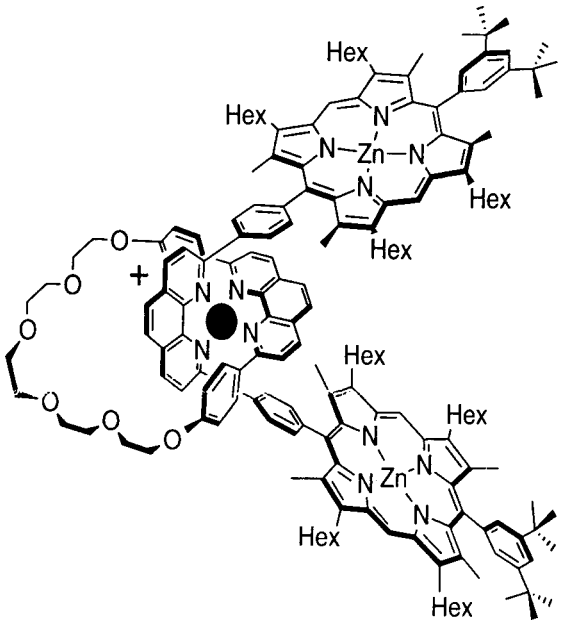

Figure 6.1

Structure of **Zn_2Cu^+**

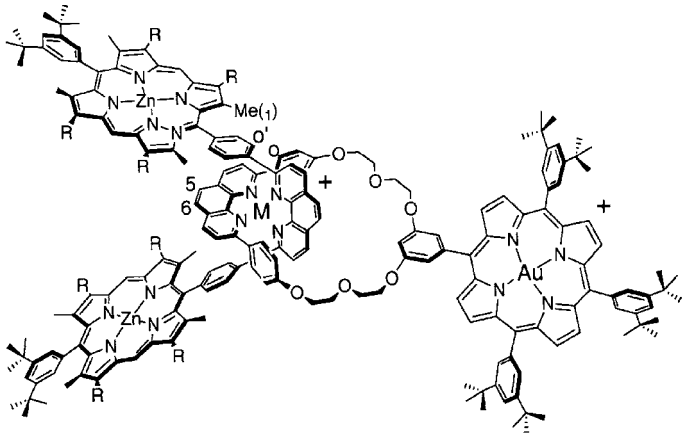

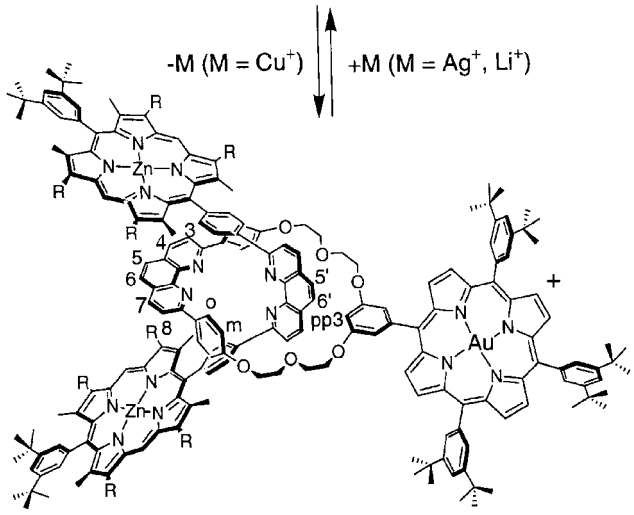

Zn_2-Au^+

Figure 6.2
Structure of the [2]-rotaxane.

The [2]-rotaxanes in figure 6.2 were designed in order to study electron transfer reactions between the ZnP and AuP^+ subunits, with special attention to the effect of the electron transfer rate of coordination of metal cations in the phenanthroline moiety. The metal cations presented in figure 6.2 are Ag^+, Cu^+

and Li^+. These metal cations changes the energy of the HOMO and LUMO levels in the phenanthrolines upon coordination, and also introduces metal centred orbitals. By the three different metal cations, the energy of the mediating link could be changed, while the rest of the molecular structure remained unchanged. (The Li^+ coordinated rotaxane was found to dissociate readily in DMF, and were excluded from the results in III and IV). Electron transfer reactions between Zn(II)- and Au(III) porphyrins have been observed in systems, where the two different porphyrins have been connected by a phenanthroline link. The electron transfer reactions were found to be mediated by the link in a superexchange mechanism[27,99,100].

Selective excitations of both the ZnP and the AuP^+ subunits of the [2] rotaxanes in figure 6.2 led to rapid electron transfer, with high quantum yields. Upon excitation of the ZnP subunit, electron transfer from the ^{1}ZnP singlet state to the ground state AuP^+ occurred, while selective excitation of the AuP^+ led to electron transfer from the ground state ZnP to the $^3AuP^+$ triplet. While the coordinated metals had very little effect on the electron transfer reactions from the ^{1}ZnP singlet, the reactions involving the $^3AuP^+$ triplet were found to vary with the coordinated metal, with a superexchange mechanism in $\mathbf{Zn_2Ag^+Au^+}$ and $\mathbf{Zn_2Au^+}$, and a sequential mechanism in the $\mathbf{Zn_2Cu^+Au^+}$ rotaxane. In figure 6.3, the observed photochemical and photophysical processes upon excitation of the different subunits are shown.

6.2 Properties of the model compounds ZnP and AuP^+

The two different porphyrins were selectively excited in the Q bands, to initially form the ^{1}ZnP or $^1AuP^+$ singlet states. The $^1AuP^+$ undergoes intersystem crossing to form the $^3AuP^+$ triplet state within a few ps [13,27,28]. The model compounds **ZnP** and $\mathbf{AuP^+}$ were used as references, and the fluorescence lifetime (2.0 ns) and intensity was measured for **ZnP .** The $\mathbf{^3AuP^+}$ triplet does not emit at room temperature, and a 2.0 ns lifetime of the $\mathbf{^3AuP^+}$ state was measured by transient absorption. The phosphorescence spectra for $\mathbf{^3ZnP}$ and $\mathbf{^3AuP^+}$ were measured at 77 K. The energies of the triplet state were taken from the blue edge of the phosphorescence spectra, while the energy of the ^{1}ZnP were taken from the midpoint of the absorption and emission 0-0 transitions. From the ground state redox potentials of the model compounds, and the measured energies of the excited states, the redox potentials for the different states were obtained.

The $\mathbf{^3ZnP}$ state was further studied by nanosecond flash photolysis. The $\mathbf{^3ZnP}$ lifetime was found to be 7. 5 μs in a deoxygenated sample, while a triplet lifetime of 6.0 μs was observed in $\mathbf{Zn_2Cu^+}$. Further, transient absorption spectra showed a time dependent spectral shift of the peak around 460 nm, with a lifetime of 100 ns of the initially formed triplet state. The observed dynamics

were interpreted as a conformational change to a non planar porphyrin, as was suggested in a recent report [29].

6.3 Electron transfer reactions upon excitation of the ZnP unit.

Upon selective excitation of the ZnP units at 575 nm, electron transfer from ^{1}ZnP to the ground state AuP^+ was observed:

$$\mathbf{Zn^1Zn - Au^+ \rightarrow ZnZn^+ - AuP^\bullet} \qquad \Delta G^0 = -0.89 \text{ eV} \qquad (24)$$

The charge transfer state reacted further in a back electron transfer to reform the ground state ZnP and AuP^+ units:

$$\mathbf{ZnZn^+\text{-}AuP^\bullet \rightarrow Zn_2 - AuP^+} \qquad \Delta G^0 = -1.25 \text{ eV} \qquad (25)$$

The forward electron transfer rate constants were obtained from both emission and transient absorption measurements. The steady state emission intensity and the observed fluorescence lifetime of the rotaxanes were compared with the model **ZnP**. The observed fluorescence decay could not be described by a single exponential function in the rotaxanes, but good quality fits were obtained by double exponential functions. In the rotaxanes a fast decay of 80 ps (30-40%) and slower 570 ps and 700 ps (60-70%) were found for $\mathbf{Zn_2Au^+}$ and $\mathbf{Zn_2Ag^+Au^+}$, respectively, while in $\mathbf{Zn_2Cu^+Au^+}$ lifetimes of 60 ps and 300 ps were observed. In $\mathbf{Zn_2Cu^+}$ the fluorescence decay was well described by single exponential lifetime of 180 ps.

Transient absorption spectra of $\mathbf{Zn_2Au^+}$, $\mathbf{Zn_2Ag^+Au^+}$ and $\mathbf{Zn_2Cu^+Au^+}$ taken at different delay times showed the formation of the charge transfer state from initial ^{1}ZnP state according to eq. 24. The transient absorption kinetics were followed at several wavelengths, and the obtained lifetimes were found to be consistent with the observed fluorescence data. Further, a transient decay corresponding to the back electron transfer (eq. 25) was seen, and lifetimes of 10 ns were obtained. The decays on the nanosecond time scale were followed by flash photolysis, which yielded lifetimes of the charge transfer state of 10 ns and 40 ns for the three rotaxanes.

In $\mathbf{Zn_2Cu^+Au^+}$ and $\mathbf{Zn_2Cu^+}$ a two step energy transfer involving $Cu^+(phen)_2$ was observed:

$$\mathbf{^1ZnZnCu^+ \rightarrow Zn_2^*Cu^+ \rightarrow {}^3ZnZnCu^+} \qquad (26)$$

In [101], energy transfer from ^{1}ZnP to $Cu(phen)_2^+$ was reported in a structurally very similar rotaxane. In **Zn_2Cu^+Au**, this process (eq. 26) competes with electron transfer (eq 24). The rate constant for the initial energy transfer was obtained from emission lifetime measurements and transient absorption of **Zn_2Cu^+**. The second energy transfer could be followed by transient absorption, as the risetime of the transient absorption due to the formation of the ^{3}ZnP state. Transient absorption traces yielded lifetimes of 650 ps of the $Zn_2{}^*Cu^+$ state in both **Zn_2Cu^+Au** and **Zn_2Cu^+**. Hence, electron transfer from the $^*Cu(phen)_2^+$ to the AuP^+ ground state was not observed. When the energy transfer processes (eq. 26) were considered in **Zn_2Cu^+Au**, the electron transfer rate constant for forward and back electron transfer (eqs. 24 and 25) were found to be similar in all three rotaxanes. The observation of biexponential behaviour in both transient absorption and emission was interpreted as the presence of several different conformations in the rotaxanes.

Thus, the coordination of metal cations did not have any large effect of the observed electron transfer rates. A slightly larger donor – acceptor distance, might explain the somewhat slower electron transfer observed in **$Zn_2Ag^+Au^+$**. In figure 6.3, the observed electron- and energy transfer processes are shown, with the energies of the different states. Electron transfer from the ^{1}ZnP state to the $Cu^+(phen)_2$ ($\Delta G^0 \approx 0$) or $Ag^+(phen)_2$ ($\Delta G^0 = -0.7$ eV) [102,103], followed by a second electron transfer to the AuP^+ unit is energetically possible. This sequential mechanism is expected to result in an increase of the observed electron transfer from the ^{1}ZnP state. The observation of similar electron transfer rate constants, and the absence of any detected intermediate charge transfer state, indicates that sequential electron transfer was not significant. Instead the mechanism is proposed to be a superexchange [6,7] in all three rotaxanes with an electron transfer pathway that do not involve the reduction of the $Ag^+(phen)_2$ or $Cu^+(phen)_2$ units.

6.4 Electron transfer reactions upon excitation of the AuP^+ unit.

Upon selective excitation of the AuP^+ unit with 528 nm light, electron transfer from the ground state ZnP unit was found to occur in **Zn_2Au^+** and **$Zn_2Ag^+Au^+$**:

$$\mathbf{Zn_2 - {}^3AuP^+ \rightarrow ZnZn^+ - AuP^\bullet} \qquad \Delta G^0 = -0.45 \text{ eV} \qquad (27)$$

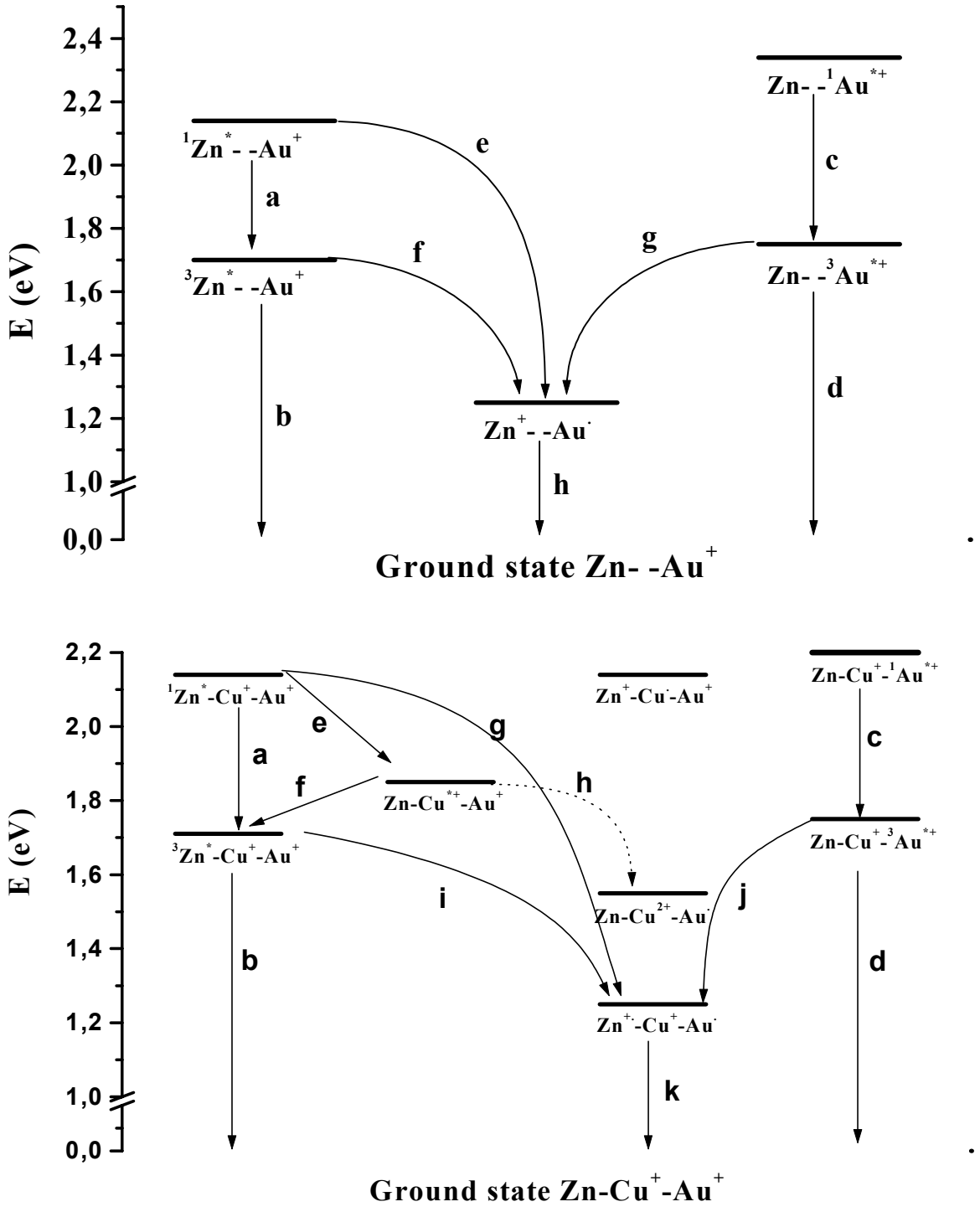

Figure 6.3
Reactions observed upon selective excitation of the ZnP and AuP^+ subunits. Top: Zn_2Au^+ and $Zn_2Ag^+Au^+$ rotaxanes. Botton: $Zn_2Cu^+Au^+$ rotaxane. From **[IV]**

The transient absorption spectra recorded at various time delays upon excitation

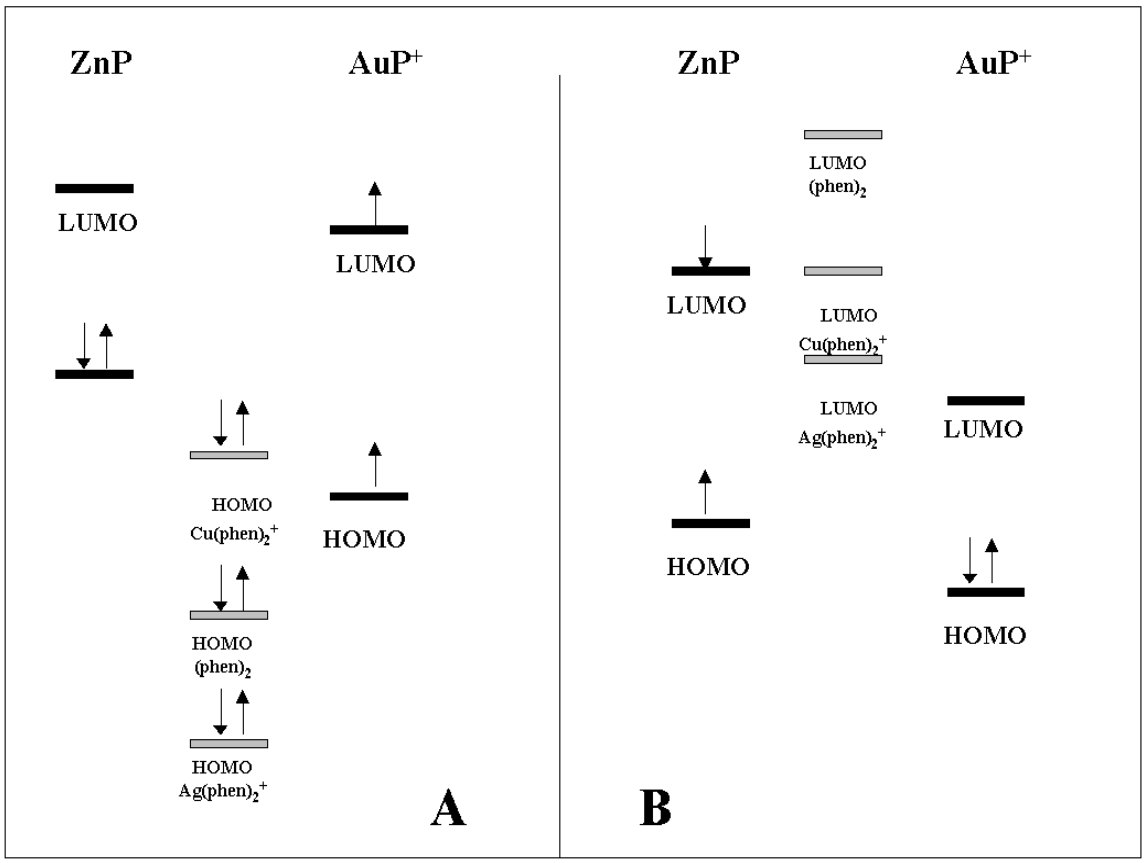

Figure 6.4. Schematic MO diagram illustrating the effect of bridge energy on through-bond electron transfer. (A) electron transfer from the ground state ZnP to the $^3AuP^+$ state (hole transfer). (B) electron transfer from the excited ^1ZnP state to the ground state AuP^+ (electron transfer)

showed the formation of the charge transfer state from the inital $^3AuP^+$ state in all rotaxanes. The kinetics of the transient absorption were analysed, and the forward electron transfer were found to occur with two rate constants, followed by a slower recombination, as in when the ZnP unit was excited. In nano second flash photolysis, the back electron transfer was followed, and the charge transfer states were found to have the same lifetimes as observed with ZnP excitation. Thus, the lifetime of the charge transfer state did not show any spin memory of the excited state which it was created from.

While the electron transfer reactions from the ^1ZnP state were almost unaffected by the presence of the coordinated metal cation in the phenanthroline moiety, the effect was evident when the electron transfer involved the $^3AuP^+$ triplet and ZnP ground states.

In **$Zn_2Ag^+Au^+$**, the forward electron transfer rate was found to be considerably larger than for the **Zn_2Au^+**, and in **$Zn_2Cu^+Au^+$** the charge transfer state was seen to be formed even faster, as presented in table 6.1.
In **$Zn_2Ag^+Au^+$** the enhanced electron transfer rate could not be explained by alternate reactions. Oxidation and reduction of the $Ag^+(phen)_2$ is endoergonic, as is also energy transfer to form the ^{1}ZnP [table2 in **IV**]. Energy transfer to form the ^{3}ZnP is exorgonic, but this process could be ruled out based on the transient absorption kinetics. In **$Zn_2Cu^+Au^+$**, a two step electron transfer mechanism was proposed:

$$\mathbf{Zn_2Cu^+\,{}^3Au^+ \rightarrow Zn_2Cu^{2+}Au^\bullet} \qquad \Delta G^0 = -0.20 \text{ eV} \qquad (28)$$

$$\mathbf{Zn_2Cu^{2+}\,Au^\bullet \rightarrow ZnZn^+Cu^+Au^\bullet} \qquad \Delta G^0 = -0.30 \text{ eV} \qquad (29)$$

The observed electron transfer reactions upon the selective excitations of the ZnP and AuP^+ units were interpreted in terms of superexchange and sequential mechanisms. In figure 6.4, the different states involved are schematically drawn, and as a simplification the links are represented as single states.

In electron transfer from the from the ground state ZnP to the $^3AuP^+$, state the electronic coupling between the donor and acceptor is increased mainly by the interaction of the HOMO of the link, according to the hole transfer mechanism [6,7] (A in figure 6.4). On the other hand, electron transfer from the ^{1}ZnP state to the ground state AuP^+ is mostly dependent on the electronic coupling of the donor and acceptor with the LUMO of the link, according to the electron transfer mechanism.[6,7].

Although the coordination of both Cu^+ and Ag^+ stabilises the LUMO of the phenanthrolines, the electron transfer rate was unaffected. The LUMO of $Cu^+(phen)_2$ is phenanthroline based, and $Ag^+(phen)_2$ has low lying orbitals on both the metal and the ligand [102,103]. When the energies of the LUMOs of the three different rotaxanes are compared, one would expect the electron transfer rate to be faster in the metal coordinated rotaxanes. The observation of similar electron transfer rates suggest that the electron transfer pathway do not involve these units.

The electron transfer to the $^3AuP^+$ state was affected by the coordination ofAg^+ and Cu^+. Oxidation by $^3AuP^+$ of both $Ag^+(phen)_2$ and the phenanthrolines in Zn_2Au^+ is endoergonic, and $Ag^+(phen)_2$ is the most difficult to oxidise. A superexchange mechanism was proposed for the electron transfer reactions in **Zn_2Au^+** and **$Zn_2Ag^+Au^+$,** where the Ag^+ cation enhances the electronic coupling

between the porphyrin donor and acceptors mainly by the coordination bonds to the two phenanthrolines. On the other hand, oxidation of the $Cu^{+}(phen)_2$ by the $^3AuP^{+}$ state is exoergonic. Therefore, the $Cu^{+}(phen)_2$ HOMO is not involved in a superexchange mechanism, but is oxidised as an intermediate in a sequential mechanism. The intermediate state was not observed, and therefore it was concluded that the second electron transfer occurs much faster than the initial.

Table 6.1
Summary of Forward Electron Transfer Rate Constants

	k_{ET} (s^{-1}) (rel. amplitudes)			
	ZnP excitation		**AuP^{+} excitation**	
Zn_2Au^{+}	1.2×10^{10} (35%)	1.3×10^{9} (65%)	1.1×10^{10} (40%)	5×10^{8} (60%)
$Zn_2Ag^{+}Au^{+}$	1.2×10^{10} (35%)	1.1×10^{10} (65%)	2.0×10^{10} (40%)	2.0×10^{9} (60%)
$Zn_2Cu^{+}Au^{+}$	1.2×10^{10} a	a	3.9×10^{10} (75%)	1.6×10^{9} (25%)

a) see text in [IV]

Acknowledgements.

First of all, I would like to thank my supervisor ***Leif Hammarström***. Your knowledge, support and enthusiasm in the scientific area is blended with a healthy sense of humour. Special thanks also to my second supervisor ***Jan Davidsson.*** Without your skills and patience, there would be no femtoseconds in this thesis. ***Everybody at the department***. You all contribute to the friendly and inspiring atmosphere. Special thanks to ***Margit,*** for the time and help with all the practical things. To ***Maja*** and ***Mats,*** for the fun meetings we had.... To the brave ***innebandy players*** *:* With your help, I got rid of some old aggressions. And got some new...To ***Anki,*** for the nice picture.

To ***Helena,*** for lots of laughs, interesting discussions and support in the not-so-good days.

To ***Nordisk Energiforskning***. For the scholarship, and the good meetings.

To ***Jouko Korppi-Tommola.***. For the good time in Finland. Kiitos!

My friends, ***Patrik, Johan, Mathias*** and all others. You remind me that there is a world outside the lab. Special thanks to Patrik who let me win the pool games.

My family in Kallinge*:* All the way, your support have helped and encouraged me.

Jenny. For making the sun shine in my life, and for being my best friend.

References

1. Deisenhofer, J.; Norris, J. R. eds, In The Photosynthetic Reaction Center, Vol. II, Academic Press, 1995
2. Balzani, V.; Scancola, F. In Comprehensive Supramolecular Photochemistry, Reinhout, D. N., Ed.; Pergamon, Oxford, 1996, Vol. 10
3. Hayes, R. T.; Wasielewski, M. R; Gosztola, D. *J. Am. Chem. Soc.* **2000**, *122*, 5563
4. Debreczeny, M. P.; Svec, W. A.; Marsh, E.; Wasielewski, M. R.; *J. Am. Chem. Soc.* **1996**, *118*, 8174
5. de Silva, A. P.; Gunaratne, H. Q. N.; Gunnlaugsson, T.; Huxley, A. J. M.; McCoy, C. P.; Rademacher, J. T.; Rice, T. E.; *Chem. Rev*. **1997**, *97*, 1515
6. McConnell, H. M.; *J. Chem. Phys.,* **1961***, 35,* 508.
7. Bixon, M.; Jortner, J. *Adv. Chem. Phys.,* **1999***, 106, ,* 35-203.
8. Newton, M. *Chem. Rev*. **1991**, *91*, 767
9. Mathews, C. K.; van Holde, K. E. In Biochemistry, 1990, Benjamin/Cummings Publishing Company.
10. Balzani, V.; Scandola, F. In Supramolecular Photochemistry, *Ellis Horwood: Chichester*, 1991
11. Wasielewski, M. R. *Chem. Rev*. **1992**, *92*, 345
12. Ali, H.; van Lier, J. E. *Chem. Rev*. **1999**, 2379
13. Kalyanasundaran, K. In Photochemistry of Polypyridine and Porphyrin Complexes, Academic Press: Lonodon, **1992**.
14. Fajer, J.; Borg, D. C.; Forman, A.; Dolphin, D.; Felton, R. H. *J. Am. Chem. Soc*. **1970**, *92*, 3451
15. Carnieri, N., Harriman, H.; *Inorg. Chim. Acta*, **1982**, *62*, 103
16. Darwent, J. R.; Douglas, P.; Harriman, A.; Porter, G.; Richoux, M.-C. *Coord. Chem. Rev*. **1982**, *44*, 83.
17. Gouterman, M. In *The Porphyrins*; Dolphin, D. (Ed), Academic Press: New York, **1978**, Vol. 3.
18. Rodriguez, J.; Kirmaier, C.; Holten, D.; *J. Am. Chem. Soc*. **1989**, *111*, 6500
19. Gouterman, M. J. Chem. Phys. **1959**, *30*, 1139
20. Kurabayashi, Y.; Kikuchi, K.; Kokubun, H.; Kaizu, Y.; Kobayashi, H. *J. Phys. Chem.* 1984, 88, 1308
21. Chosrowjan, H.; Tanigichi, S.; Okada, T.; Takagi, S.; Arai, T.; Tokumaru. *Chem. Phys. Lett.* **1995**, *242*, 644
22. Bajema, L.; Gouterman, M.; Rose, C. B.; J. Mol. Spectrosc. **1971**, *39*, 421
23. Gurzadyan, G. G.;Tran-Thi, T.-H.; Gustavsson, T. *J. Chem. Phys*. **1998**, *108*, 385
24. Akimoto, S.; Yamazaki, T.; Yamazaki, I.; Osuka, A. *Chem. Phys. Lett*. **1999**, *309*, 177
25. Vacha, M.; Machida, S.; Horie, K. *J. Phys. Chem.* **1995**, *99*, 13163
26. Tsvirko, M.P.; Stelmakh, G. F.; Pyatosin, V. E.; Solovyov, K. N.; Kachura, T. F. *Chem. Phys. Lett.* **1980**, *73*, 80
27. Brun, A. M.; Harriman, A.; Heitz, V.; Sauvage, J.-P. *J. Am. Chem. Soc*. **1991**, *113*, 8657
28. Antipas, A.; Dolphin, D.; Gouterman, M.; Johnson, E. C. *J. Am. Chem. Soc.* **1978**, *100*, 7705
29. Knyukshto, V.; Zenkevich, E.; Sagun, E.; Shulga, A.; Bachilo, S. *Chem. Phys. Lett.* **1998,** *297,* 97.
30. Yamaguchi, S.; Hamaguchi, H.-O. *Applied Spectrosc.* **1995**, *49*, 1513
31. Marcus, R. A. *J. Chem. Phys.* **1956**, *24*, 966
32. Marcus, R. A. *J. Chem. Phys*. **1956**, *24*, 979

33. Marcus, R. A. *Ann. Rev. Phys. Chem*. **1964**, *15*, 155
34. Marcus, R. A.; Sutin, N.; *Biochim. Biophys. Acta*, **1985**, *811*, 265
35. Levich, V. O. *Adv. Electrochem. Electrochem. Eng. 4, 249 (1966)*
36. Barbara, P. F.; Meyer, T. J.; Ratner, M.; *J. Phys. Chem.* **1996**, *100*, 13148
37. Bixon, M.; Jortner, J. *J. Chem. Phys*. **1997**, *107*, 5154
38. Hush, N. S. *Prog. Inorg. Chem.* **1967**, *8*, 391
39. Newton, M.; *Chem. Rev.* **1991**, *91*, 767
40. Jortner, J.; Bixon, M.; *Adv. Chem. Phys.*, **1999**, *106*, 35
41. Bolton, J. R.; Archer, M. D. In Electron Transfer in Inorganic, Organic and Biological Systems; Bolton, J. R., Mataga, N.; McLendon, G. (Eds.) Advances in Chemistry Series 228; American Chemical Society, Washington DC, 1991, Chapter 2
42. Closs, G. L.; Calcaterra, L. T.; Green, N. J:, Penfield, K. W.; Miller, J. R. *J. Phys. Chem*. **1986**, *90*, 3673
43. Johnson, M. D.; Miller, J. R.; Green, N.; Closs, G. L. *J. Phys. Chem.* **1989**, *93*, 1173
44. Closs, G. L.; Miller, J. R.; *Science*, **1988**, *240*, 440
45. Suppan, P. *Top. Curr. Chem.* **1992**, *163*, 97 (and references therein)
46. Rehm, D.; Weller, A. *Israel J. Chem.* **1970**, *8*, 259
47. Brunschwig, B. S.; Ehrenson, S.; Sutin, N.*; J. Phys. Chem*. **1986,** *90*, 3657
48. Bixon, M.; Jortner, J. *J. Phys. Chem.* **1991***,95,* 1941
49. Jortner, J. *J. Chem. Phys.* **1976**, *64*, 4860
50. Rips, I.; Jortner, J.; *J. Chem. Phys.* 1987, *87*, 2090
51. Jortner, J.; Bixon, M.; *J. Chem. Phys.* 1988, *88*, 167
52. Vergelt, F. J.; Koehorst, R. B. M.; Schaafsma, T. J.; Lambry, J. –C.; Marin, J.-L.; Johnson, D. G.; Wasielewski, M. R. *Chem. Phys. Lett*. **1991**, *182*, 107
53. Oevering, H; Paddon-Row, M. N.; Heppener, M.; Oliver, A. M.; Cotsaris, E.; Verhoeven, J. W.; Hush, N.S. *J. Am. Chem. Soc.,* **1987***,109*, 3258.
54. Helms A.; Heiler D.; McLendon, G *J. Am. Chem. Soc.,* **1992***,114,* 6227. (d)
55. Finckh P.; Heitele, H.; Volk, M.; Michel-Beyerle, M. E. *J. Phys. Chem.,* **1988***, 92,* 6584.
56. Ribou, A. C.; Launay, J. P.; Takahashi, K.; Nihira, T.; Tarutani, S.; Spangler, C. W. *Inorg.Chem.,***1994***,33,*1325
57. Wasielewski, M. R.; Johnsson, D. G.; Svec, W. A.; Kersey, K. M.; Cragg, D. F.; Minsek, D. W. In *Photochemical Energy Conversion;* Norris, J. R., and Meisel, D. (eds), Elsevier*,* **1989**.
58. Beratan, D. N.; Betts, J. N.; Onuchic, J. N. *Science,* **1991***, 252,* 1285.
59. Beratan, D. N.; Onuchic, J. N.; Winkler, J. R.; Gray, H. B. *Science,* **1992**, *258,* 1740.
60. Gray, H.B.; Winkler, J. R. *Ann. Rev. Biochem.* **1996,** *65,* 537.
61. Winkler, J.R.; Gray, H.B. *J. Biol. Inorg. Chem.2, **1996**, 1,* 221-225.
62. Winkler, J. R.; Gray, H. B.; *J. Biol. Inorg. Chem.2,* **1997***, 3,* 399.
63. Moser, C.C.; Keske, J. M.; Warncke, K.; Farid, R.S.; Dutton,L. *Nature,***1992** *355,* 796.
64. Page, C. C.; Moser, C. C.; Xiaoxi, C.; Dutton, L. *Nature*, **1999,** *402*, 47-52,
65. McConnell, H. M.; *J. Chem. Phys.,* **1961***, 35,* 508.
66. Sutin, N. *Adv. Chem. Phys*. **1999**, *106*, 7, and references therein
67. Wasielewski, M. R. *Chem. Rev.* **1992**, *92*, 435
68. Gust, D.; Moore, T.; *Acc. Chem. Res.* **1993**, *26*, 198
69. Kurreck, H.; Huber, H.; *Angew. Chem. Int. Ed. Engl.* **1995**, *34*, 849
70. Harriman, A.; Sauvage, J.-P. *Chem. Soc. Rev*. **1996**, 41
71. Head, N. J.; Thomas, J.; Shephard, M. J.; Paddon-Row, M. N.; Bell, T. D. M.; Cabral, N. M.; Ghiggino, K. P. *J. Photochem. Photobiol. A: Chem.* **2000**, *133*, 105
72. Springs, S. L.; Gosztola, D.; Wasielewski, M. R.; Král, V.; Andrievsky, A.; Sessler, J. *J. Am. Chem. Soc*. **1999**, *121*, 2281

73. Wiederecht, G. P.; Niemczyk, M. P.; Svec, W. A.; Wasielewski, M. R.; *J. Am. Chem. Soc.* **1996**, *118*, 81
74. Osuka, A.; Noya, G.; Taniguchi, S.; Okada, T.; Nishimura, Y.; Yamazaki, I.; Mataga, N. *Chem. Eur. J.* **2000**, *6*, 33
75. Tsue, H.; Imahori, H.; Kaneda, T.; Tanaka, Y.; Okada, T.; Tamaki, K.; Sakata, Y. *J. Am. Chem. Soc.* **2000**, *122*, 2279
76. Kilin, D.; Kleinekathöfer, U.; Schreiber, M. *J. Phys. Chem. A*. **2000**, *104*, 5413
77. Flamigni, L.; Armaroli, N.; Barigilletti, F.; Balzani, V.; Collin, J.-P.; Dalbavie, J.-O.; Heitz, V.; Sauvage, J.-P.; *J. Phys. Chem. B* **1997**, *101*, 5936
78. Harriman, A.; Hissler, M.; Trompette, O.; Ziessel, R.; J. Am. Chem. Soc. 1999, 121,2516
79. Rodgers, M. A. J.; Logunov, S. L. *J. Phys. Chem*. **1992**, *96*, 8697
80. Yu, H. Z.; Baskin, J. S.; Steiger, B.; Wan, C. Z.; Anson, F. C.; Zewail, A. H.; *Chem. Phys.*
Lett. **1998**, *293*, 1
81. Frey, W.; Klann, R.; Laerner, F.; Elsasser, T.; Baumann, E.; Futscher, M.; Staab, H. A.; *Chem. Phys. Lett.* **1992**, *190*, 567
82. Heitele, H.; Pöllinger, F.; Häberle, T.; Michel-Beyerle, M. E.; Staab, H. A.; *J. Phys. Chem*. **1994**, *98*, 7402
83. Wynne, K.; LeCours, S.; Galli, C.; Therien, M. J.; Hochstrasser, R. M.; *J. Am. Chem. Soc.* **1995**, *117*, 3749
84. Shibata, Y.; Chosrowan, H.; Mataga, N.; Osuka, A. *J. Lumin*. **2000**, *87-89*, 757
85. Zenkevich, E. I.; Shulga, A. M.; Bachilo, S. M.; Rempel, U.; von Richthofen, J.; von Borczyskowski, Ch. *J. Lumin.* **1998**, *76&77*, 354
86. Kaneko, Y.; Nishimura, Y.; Arai, T.; Sakuragi, H.; Tokumaru, K.; Matsunaga, D.; *J. Photochem. Photobiol. A : Chem*. **1995**, *89*, 37
87. Vlcek, Jr. A. CHEMTRACTS – Inorg. Chem. **1999**, *12*, 863
88. Brun, A. M.; Harriman, A.; Hubig, S. M.; *J. Phys. Chem*. **1992**, *96*, 8697
89. Wiederrecht, G. P.; Svec, W. A.; Wasielewski, M. R.; *J. Am. Chem. Soc.* **1999**, *121*, 7726
90. Stern, O.; Vollmer, M. *Physik. Z.* **1919**, *20*, 183
91. Watanabe, T.; Honda, K. *J. Phys. Chem*. **1982**, *86*, 2617
92. Sven Larsson., Hyper Chem ^{TM} calculations, unpublished results.
93. In the calculations in [92], a value of λ_i of ≈0.7 eV was obtained, with a main contribution from the methyl viologen. If this value is taken together with the estimated λ_o, a value of λ closer to the value of obtained in [79] .
94. Stratt, R. M.; Maroncelli, M.; *J. Phys. Chem.* **1996**, *100*, 12981
95. Neta, P. *J. Phys. Chem*. **1981**, *85*, 3678.
96. Abou-Gamra, Z.; Harriman, A.; *J. Chem. Soc. Faraday Trans. 2* **1986**, *82*, 2337.
97. Fajer, J.; Borg, D. C.; Forman, A.; Dolphin, D.; Felton, R. H. *J. Am. Chem. Soc*. **1970**, *92*,3451.
98. Mulazzani, Q. G.; Emmi, S.; Fuochi, P. G.; Hoffman, M. Z.; Venturi, M. *J. Am. Chem. Soc.* **1978**, *100*, 981.
99. Brun, A. M.; Atherton, S. J.; Harriman, A.; Heitz, V.; Sauvage, J.-P. *J. Am. Chem. Soc*. **1992**, *114*, 4632
100. Chambron, J.-C.; Harriman, A.; Heitz. V.; Sauvage, J.-P.*; J. Am. Chem. Soc*. **1993**, *115*, 7419
101. Flamigni, L.; Armaroli, N.; Barigelletti, F.; Chambron, J.-C.; Sauvage, J.-P.; Solladie, N. *New J. Chem.* **1999***, 23,* 1151
102. Dietrich-Buchecker, C.; Sauvage, J.-P.; Kern, J.-M. *J. Am. Chem. Soc*. **1989**, *111*, 7791.
103. Billon, M.; Divisia-Blohorn, B.; Kern, J.-M.; Sauvage, J.-P. *J. Mater. Chem.* **1997**, *7*, 1169.

Errata list.

Page 12, bottom.
The description of transitions corresponding to the Q and B bands has been wrongly simplified. Both the B and Q transitions involve the a1u and a2u orbitals. The transition dipoles from a1u to eg and a2u to eg adds in a constructive way in the B transition, while the transition dipoles add in a destructive way in the Q transitions.

Page 14. Line 4 from bottom: " with a quantum yields typically..."
should be " with quantum yields typically..."

Page 19, below equation 5:
" ...passing through two the sample..." should be "...passing through the sample.."

Page 20, line 6: "...the attenuation be less than...." should be "....the attenuation will be less than..."

Page 23, section 3.4 : " Transient absorption spectra were obtained with a CCD"
should be: "Transient absorption spectra were obtained with a charge coupled device, CCD."

Page 24, Line 6 below figure 3.5: "... could be calculated if the refractive index in known for all....."
should be "...be calculated if the refractive index and material thickness is known for all...."

Page 28, Figure 4.1, Bottom left : should be $\Delta G = -\lambda$

Page 33. last line in section 2: "...and a proposed sequential mechanism is proposed"
should be: "...and a sequential mechanism is proposed."

Page 43. Figure 5.5 should be Figure 5.4
Line 4 from top: Figure 5.6 should be 5.4

Page 45 Figure 5.7 should be Figure 5.5

Page 44 , line 5 from bottom: Figure 5.7 should be Figure 5.5

Paper IV

Figure 12 and 13 have been wrongly numbered. Figure 12 is Figure 13, and Figure 13 is Figure 12.

Page 57; Figure caption 13. The rotaxane given is $\mathbf{Zn_2\text{-}Ag^{+}\text{-}Au^{+}}$. This should be $\mathbf{Zn_2\text{-}Au^{+}}$**.**

Paper V.

Page 1: Line 11 from bottom: "di methyl chloride" should be "dichloromethane"
Page 2: Results section 1: The potentials are given as vs SCE.
Results section 1, The transient absorption spectra for the reduced $Ru(bpy)_3^{+}$ unit was recorded for the reference compound L- $Ru(bpy)_3^{2+}$
Page 5: section 4, line 9: "strong" should be "rapid".
Page 7: Ref 6 is Anoxygenic Photosynthetic Bacteria; Blankenship, R. E.; Madigan, M. T.; Bauer, C. E. (Eds.) Kluwer Academic Publishers; Dordrecht, 1995.
Figure 3: (Legend) S1 and T1 states are with $Ru(bpy)_3^{2+}$, CT should be with $Ru(bpy)_3^{+}$, and Ru* should be $^3Ru(bpy)_3^{2+}$
Figure 7: The lifetime of the S_2 state should be 2.4 ps.